Design Evaluation of Resilient Deep Space Habitats with a Numerical Habitat Simulator

Seungho Rhee * and Davide Ziviani†
Ray W. Herrick Laboratories, School of Mechanical Engineering, Purdue University, West Lafayette, IN, 47907-2099

To advance long-term human exploration of the Moon and beyond, developing resilient deep space habitats capable of autonomous operation during both manned and unmanned periods is crucial. Earth-based buildings allow for immediate maintenance and access to external resources. In contrast, damages and disruptions to deep space habitats (e.g., micrometeorite impacts, moonquakes, internal fire, sensor failures, power outages, etc.) will be extremely challenging to address due to the unique conditions in space. Given the inevitability of such disturbances, resilient designs would not only minimize the likelihood of system failure, but also mitigate overall risks. Therefore, design evaluations of resilient deep space habitats under various potential disturbances at the early design phase are necessary before deployment. This paper introduces a resiliency-based design evaluation framework for deep space habitats, using a deterministic structural-based habitat simulator (HabSim) along with a performance-based quantitative resilience assessment. HabSim generates various habitat behaviors to assess the performance and resilience of designs of the habitat through known resilience assessment metrics. An illustrative case study is included to demonstrate the effectiveness and capabilities of this evaluation framework.

Nomenclature

A	=	area, m^2
c_p	=	specific heat at constant pressure, $kJ/kg-K$
$\mathrm{d}t$	=	time step, s
E	=	total energy, kJ
g	=	gravitational acceleration, m/s^2
G_s	=	direct normal solar radiation, W/m^2
h	=	specific enthalpy, kJ/kg
k_m	=	porous media permeability, m^2

*Ph.D. Student, School of Mechanical Engineering, West Lafayette, IN, 47907-2099; rhee18@purdue.edu (Corresponding Author).
†Associate Professor, School of Mechanical Engineering, West Lafayette, IN, 47907-2099.

K_v = valve flow coefficient, -

l = extended length of the radiator fin, m

m = mass, kg

$\dot{m}$ = mass flow rate, kg/s

P = pressure, kPa

PS = Performance state, -

$\dot{Q}$ = heat transfer rate, kW

r = radius of the tube, m

SV = state variable, $^\circ C$, kPa, etc.

T = temperature, $^\circ C$

u = specific internal energy, kJ/kg

U = internal energy, kJ

U_f = convective heat transfer coefficient, kW/m^2K

v = mean velocity, m/s

V = volume, m^3

w = half thickness of the radiator fin, m

w_r = weight factor of the severity range, -

$\dot{W}$ = rate of the boundary work done, kW

z = height at which mass transfer through the boundary, m

ρ = density, kg/m^3

λ = thermal conductivity, $kW/m-K$

μ = dynamical viscosity, $Pa-s$

ε = emissivity, -

α = absorptivity, -

ΔP = pressure drop or difference, kPa

θ = Latitude, $^\circ$

δ = thickness of the dust layer, m

γ = area fraction of dust cover, -

η_r = efficiency of the radiator fin, -

$\mathcal{H}$ = Heaviside step function, -

$\mathcal{R}$r = recovery resilience metric, s

$\mathcal{R}$loss = resilience loss metric, s

Subscripts

COE = conservation of energy equation

COM = conservation of mass equation

conv = convection

cv = control volume

d = dust

e = outlet

f = internal fire or fluid

hg = heat gain

i = inlet

leak = leakage

r = radiator fin surface

rel = relief

sup = supply

t = air storage tank

v = valve

w = interior wall

I. Introduction

For decades, there has been a persistent endeavor to establish a sustainable human presence in space. The Mir space station lasted 15 years, which was three times longer than its planned mission duration [1]. The International Space Station (ISS) began its service in 1998 as an international space research laboratory [2] and has hosted more than 270 astronauts for extended periods of time. As the ISS is aging, NASA's next vision is to establish a more permanent presence on the Moon (both in orbit and on its surface) and eventually on Mars. Building space habitats is one of the key steps in the Artemis program led by NASA to provide a base camp for astronauts. Furthermore, these habitats will act as a communication hub for the Earth, research laboratories, and testbeds for future planetary missions [3]. Habitats will allow scientific research and technology development in various fields of engineering and science. For example, habitats can facilitate the study of astronomy, physics, physiological and psychological human health in space [4, 5]. It also enables the development of structural design, facilities and equipment, power generation, energy storage, Environmental Control and Life Support Systems (ECLSS), and robotic operating systems on the Moon and in preparation for Mars missions [6–8]. Particularly in lunar habitats, important areas of investigation including using lunar regolith as a source of oxygen and water supply [9, 10], the Moon's geology [11], lunar space weather [12, 13],

lunar base operations [14, 15], and lunar navigation [16]. These research efforts are part of the preparation for further deep space exploration beyond Mars [17].

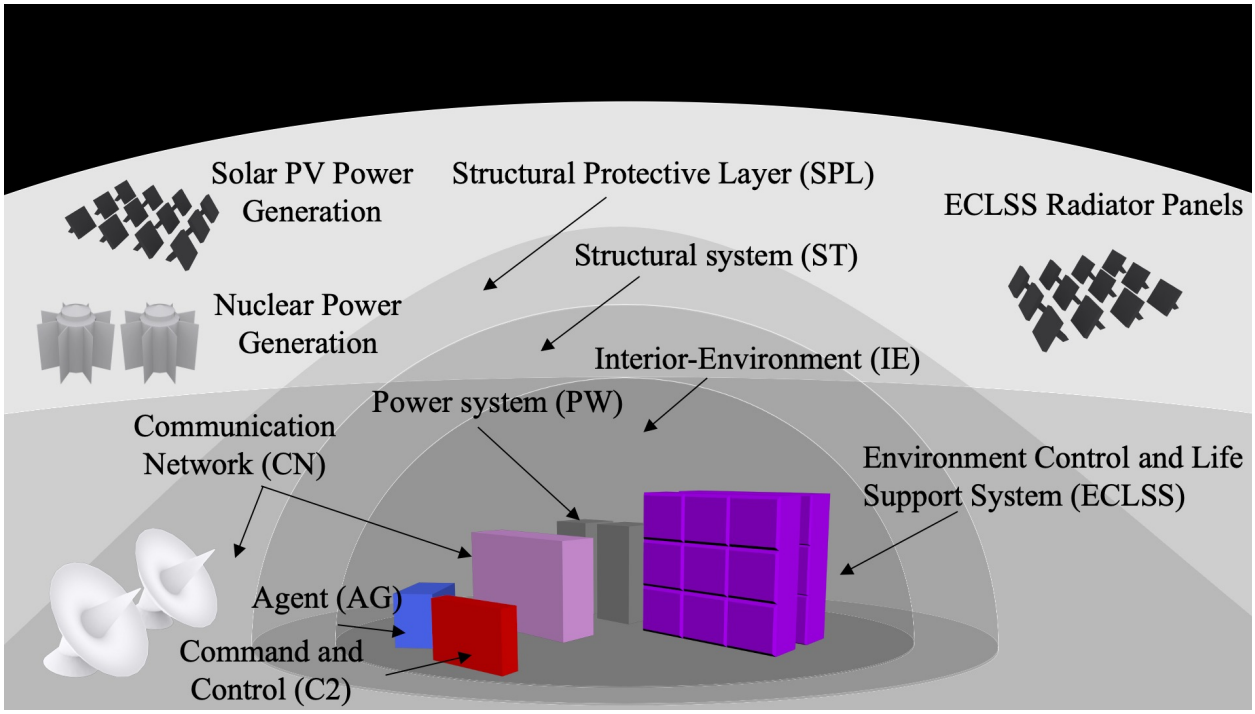

Fig. 1 A preliminary conceptual design of a lunar habitat.

To fulfill their designed purposes and required functionalities, deep space habitats need to be a system of systems (SoSs), which involves the integration of complex subsystems that operate independently and interact with each other in a synergistic way to enable various functionalities that cannot be achieved by a single independent subsystem [3, 18–20]. Resilient Extra-Terrestrial Habitat Institute (RETHi)* has conceptualized different designs of deep space habitats, specifically habitats considering lunar environmental conditions, as graphically illustrated in Fig. 1 [21]. The Interior-Environment (IE) represents an inhabitable space within the habitats with various electrical equipment and devices. Its conditions, such as temperature, pressure, and humidity, must be maintained at the desired level for the safety of astronauts, equipment, and scientific research samples. The Structural System (ST) comprises multiple layers of advanced materials designed to shield habitats from harsh lunar conditions and physical threats such as moonquakes and micrometeorites, serving as an inner protective layer. The Structural Protective Layer (SPL) serves as an outer covering for the habitats and is designed to insulate them from severe thermal conditions in the surrounding environment. This layer is made of lunar regolith, as it is a good insulator with a low thermal conductivity of approximately $1.15 \times 10^{-3}\,\mathrm{W\,m^{-1}\,K^{-1}}$ [22]. The Power System (PW) consists of batteries and converters in the habitats, a solar photovoltaic (PV) power generator, and a nuclear power generator in the exterior environment to be able to generate

*The Resilient Extra Terrestrial Habitat institute webpage: https://www.purdue.edu/rethi/

enough energy and store it during a lunar day to survive during a lunar night. ECLSS in ISS has numerous subsystems, including Atmosphere Control and Supply (ACS), Atmosphere Revitalization System (ARS), Temperature and Humidity Control (THC), Water Recovery and Management (WRM), as well as Vacuum System (VS) [23]. To communicate with ground control on Earth, habitats need a Communication Network (CN). Moreover, habitats must be operable not only during manned mission periods, but also during periods in the absence of a crew by incorporating Command and Control (C2). Lastly, intelligent robots, named Agent (AG), will properly maintain, repair, and recover any damaged equipment. It is envisioned that future habitat will feature multiple subsystems to meet performance and standard requirements.

Due to the harsh environmental conditions in space (e.g., near-vacuum, intense solar radiation, extremely fluctuating surface temperatures, etc.), deep space habitats will be subjected to numerous potential disturbances. Given that these habitats are expected to serve for over a decade and will contain multiple interconnected subsystems to perform complex functionalities, habitats will inherently feature various uncertainties and unexpected changes in system operation. Moreover, disruptive events, such as micrometeorite impacts and moonquakes, can affect the reliability of habitats either directly or indirectly; disruptive events can damage habitats directly, while extreme environmental conditions will accelerate habitat degradation. Additionally, space habitats will not be easily receiving immediate support and maintenance from Earth or low orbit stations. Consequently, it is important for habitats to be resilient and sustainable for long-term missions in these severe conditions of space [24, 25]. This necessity entails that habitats should integrate multiple essential subsystems that need to function consistently even with some level of degradation and be recovered quickly due to the crucial roles they play.

Many researchers in various fields of engineering and science have investigated and evaluated the resilience of a system and SoSs, proposing assessment methodologies and suggesting resilience enhancement strategies, as summarized in Table 1. To enhance the resilience of systems, designers and engineers can have two improvement approaches: 1) refining system designs through adjustment in configurations, capacities, redundancy [26–32], and 2) optimizing necessary operating strategies including optimal repair rates and sequences, setpoint control algorithm, partial repairs [31, 33–37]. For space applications, specifically deep space habitats, modifying system design configurations might not provide sufficient resilience enhancement to respond to challenging space environments; system operating strategies, including repair and recovery actions, must be integrated into overall systems' designs to support habitats that can withstand and respond to disruptive events to reduce overall risk instead of avoiding potential failures [38]. However, evaluating the resilience of deep space habitats and exploring the required intervention of them have been studied little. Some design configurations of ECLSS and its optimal control algorithms have been investigated at the system-level, not at the habitat-level [28, 30, 36]. Furthermore, each subsystem will be closely coupled with others in future space habitats, so having a habitat-level simulation model with flexibility of design and operating strategy modifications is required to investigate habitat behaviors and responses before, during, and after disruptive events.

To overcome current research gaps and further the study of resilient deep space habitats, this paper introduces

Table 1 Summary of literature review on resilience evaluation and enhancement.

Year	Authors	Application	Disruption	Resilience improvement approach
2008	Castet and Saleh [26]	Spacecraft	Degradation	System design
2010	Cimellaro *et al.*[33]	Health care facility	Earthquake	Operating strategy
2012	Henry and Ramirez-Marquez [34]	Road network	Rock slide / flood	Operating strategy
2015	Gu *et al.* [27]	Manufacturing systems	Machine degradation	System design
2016	Adjetey-Bahun *et al.* [35]	Transportation systems	Excessive passengers	Operating strategy
2018	Balchanos *et al.* [28]	Advanced Life Support system	Life support risks	System design
2018	Moslehi and Reddy[29]	Integrated energy systems	Component failures	System design
2018	Matelli and Goebel [30]	ECLSS	Functional failures	System design
2019	Xing *et al.* [31]	Sensor network system	Sensor malfunction	System design & Operating strategy
2021	Zhang *et al.* [32]	Cooling strategies	Heat wave / power outages	System design
2021	Rines *et al.* [36]	ECLSS	Degradation	Operating strategy
2022	Abbasnejadfard, *et al.* [37]	Urban transportation network	Earthquake	Operating strategy
-	This work	Deep space habitats	Potential disturbances	System design & Operating strategy

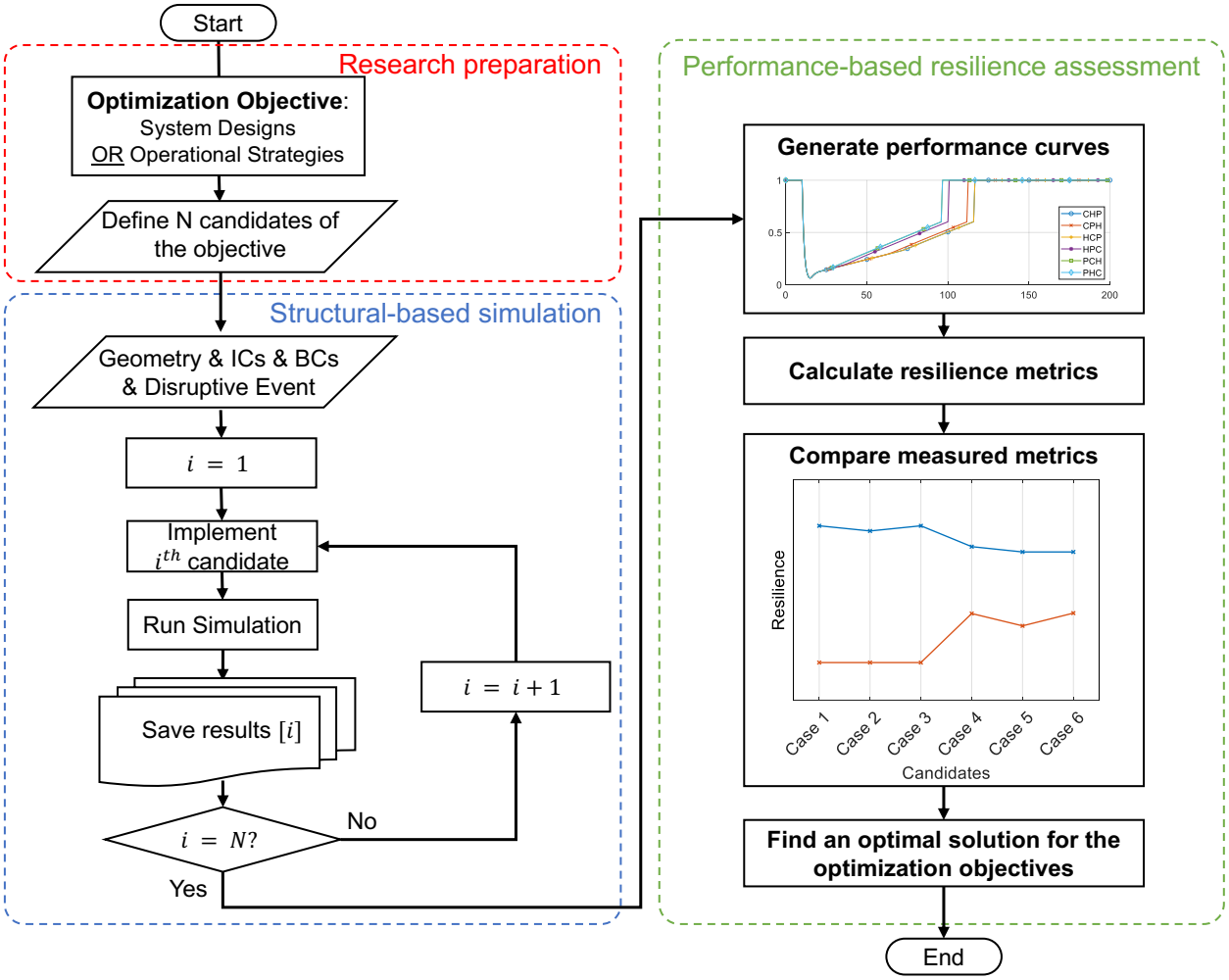

Fig. 2 Flow diagram of the proposed framework.

a comprehensive and generic resilience-based design evaluation framework as illustrated in Fig. 2. The framework consists of a structural-based simulation model and a performance-based resilience assessment. RETHi has developed

a deep space habitat simulator, HabSim, which integrates multiple subsystems, including SPL, ST, IE, ECLSS, and more [21, 38]. This simulator enables users to understand and evaluate habitat behaviors under various conditions, employing different design configurations and operating strategies. HabSim is modularized at subsystem-level, allowing for easy modification and the replacement of subsystem modules with new numerical components. This modeling approach enables the simulator to produce data across component, subsystem, and habitat levels due to its distinct architecture. Furthermore, researchers can input various interventions into HabSim, such as repair sequence, repair rate, and resource availability. Hypothetically defined disruptive events in HabSim can change habitat behaviors to allow researchers to investigate habitat responses before and after events and optimize habitat design or operating strategies to assess their resilience. In this paper, the overall architecture of the simulation model is introduced, along with details of two subsystem modules, IE and ECLSS. Additionally, the performance-based resilience assessment is discussed to demonstrate the capability of the resiliency-based design evaluation framework. Lastly, an illustrative case study is conducted to demonstrate the proposed framework.

II. A Structural-based Simulation Model

Due to the unique challenges of the space environment, an in-depth investigation of deep space habitats is essential to understand their complex dynamical behaviors including responding to disturbances and potential uncertainties during the early design phase. HabSim, a deterministic structural-based simulation model, is developed to replicate realistic habitat configurations by numerically modeling and integrating each component, enabling the investigation of the system's behaviors and performances under various conditions [21]. In this section, the architecture of HabSim and its features are described. Furthermore, two of the eight subsystem modules are introduced, which are mainly used for an illustrative case study provided in this paper. More detailed and general information on HabSim is provided in Ref.[21].

A. HabSim: Modular Coupled Virtual Testbed

HabSim is a modular coupled virtual testbed in Simulink (MATLAB-based graphical programming environment) [39], as described in Fig. 3. This model simulates the behaviors and responses of a deep space habitat with initial and boundary conditions, disturbance input, and predefined intervention (i.e., agent actions), including repair and recovery action strategies. Based on a deep space habitat design conceptualized within RETHi and illustrated in Fig. 1, multiple subsystems are developed independently and integrated with each other in a single Simulink model. The Simulink model consists of nine coding blocks, including Structural Protective Layer (SPL), Structural System (ST), Interior-Environment (IE), Environmental Control and Life Support System (ECLSS), Power System (PW), Agent (AG), Communication Network (CN), and Disturbance Block (DB), as well as Coordinate Block (CB) which collects and distributes data from one block to another. The SPL, ST, IE, ECLSS, and PW represent the physical structure, equipment, or space within the habitat, while the CN and DB serve as a communication tool to ground control on Earth

and a disturbance generator, respectively. The AG indicates an intelligent robot that can be activated based on predefined action strategies to repair and recover damaged components.

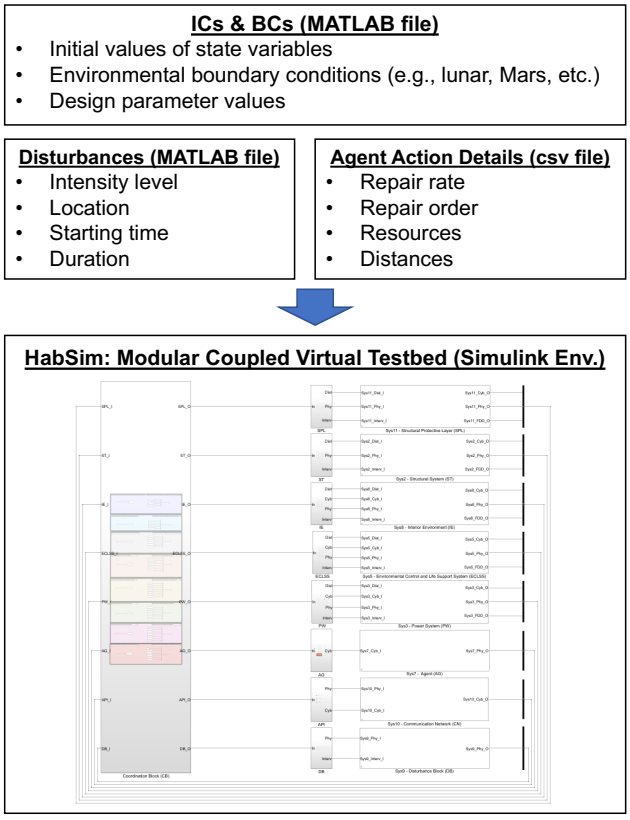

Fig. 3 Overview of simulation architecture of HabSim.

This architecture of the simulation model provides significant benefits to users and researchers; Users can run a simulation with some or all the subsystems depending on their research purpose and scope by replacing unnecessary subsystem blocks with constant boundary conditions. This modeling approach allows for simplicity of study and faster simulation running time by reducing computational cost. For example, researchers can deactivate the SPL and ST modules and provide constant boundary conditions for the IE if they are only interested in the interior environment of the habitat with ECLSS, assuming constant interior wall surface temperature [40]. Furthermore, engineers and designers can investigate different habitat design configurations by either modifying or replacing the existing subsystem block with a new block in which they have an interest. For instance, engineers can develop a new ECLSS module with different configurations or capacity of the system and replace the previous block with the new one to compare their efficiency. In addition, decision makers, including designers, engineers and others who will make a decision in the early design phase, can explore optimal repair and recovery action strategies by implementing modifying input files of the AG action policies. Lastly, researchers can adjust the initial and boundary conditions to study the habitat at a specific location, such as the surface of the Moon and orbit of Mars.

HabSim is a physics-based real-time deterministic simulation model with hypothetically designed disturbances. The primary purpose of HabSim is to investigate the performance and responses of habitats to changes or damage events with various system configurations and operating strategies during the early design phase [25]. Utilizing physics equations and featuring intermediate fidelity, HabSim provides sufficiently realistic and complex trends in habitat behaviors and performances, even before deployment. Moreover, this model offers researchers the opportunity to enhance the resilience of future habitat designs, thereby enabling long-term space exploration. The deterministic nature of HabSim makes it particularly useful for worst-case analysis and is well-suited for assessing specific types and degrees of disruptions, despite neglecting randomness and uncertainties due to limited information. These capabilities enable researchers to evaluate habitat designs and improve resilience by effectively preparing for potential risks. This investigation of efficient risk management can be accomplished through adequately realistic simulation results, which are not achievable with fast, low-fidelity simulation models. Currently, HabSim is used to analyze habitat behaviors in various damage scenarios over certain periods. However, the results are significantly meaningful as they can be consistently utilized in future habitats to address various repeated unforeseen changes or disruptive occurrences.

HabSim is a comprehensive simulator with numerous capabilities and features. This paper focuses mainly on the IE and ECLSS modules to investigate habitat performances due to a disruptive event. Lunar environmental conditions and corresponding material properties are implemented in the model to investigate lunar habitats. The damage propagation network indicating cascading effects due to disruptive events is illustrated in Fig. 4.

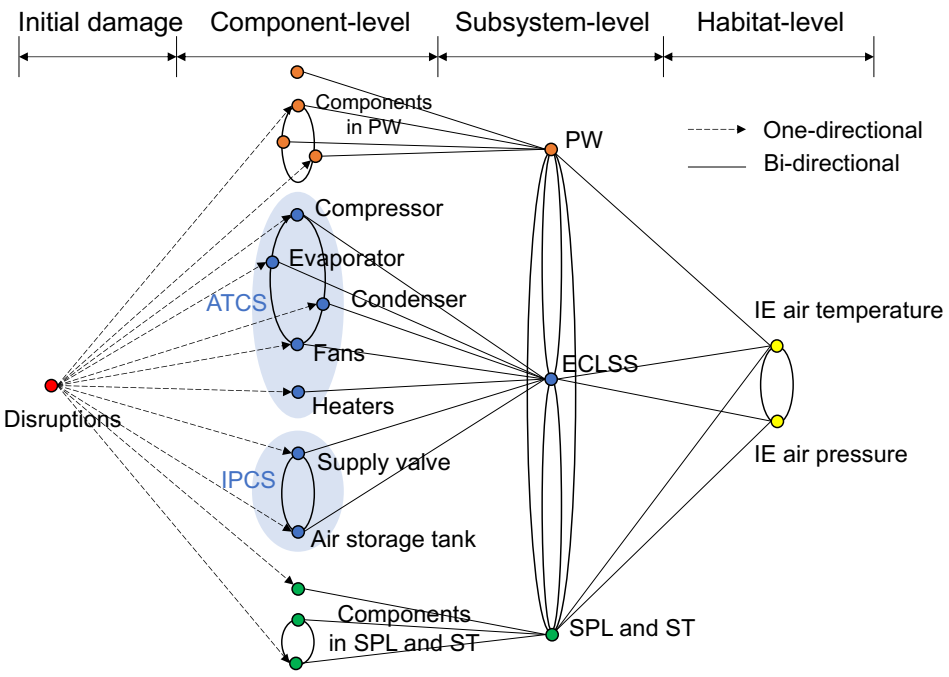

Fig. 4 Simplified network diagram of HabSim damage propagation and cascading effects.

B. Module 1: Interior-Environment

The IE module represents an interior habitable space within a multi-zonal lunar habitat. The air temperature, pressure, and rate of change of these variables in the interior of the habitat are tracked in real-time using physics equations. The IE interacts with numerous other habitat subsystems, including the thermal and pressure control systems in the ECLSS, the interior wall surface temperature and the radius of a potential leak in the ST, the heat gain from the PW and the ECLSS, and the disturbance data from the DB. In addition, the IE has its own heat sources, which is the heat from the crew. To connect the zones, a pocket door is placed in the center of a wall between the zones. Normally, the pocket door is open so that crew members can enter. The door can be closed for safety purposes to isolate a zone that has been damaged as a result of a disruption scenario (e.g., a meteorite impact and internal fire) from the other health zones. When this door is open, the IE model can detect air convection through it. In contrast, air convection is cut off and removed from the governing equations when the door is closed.

A quasi-static zero-dimensional lumped model approach has been developed to predict indoor air temperature and pressure within each zone while accounting for multiple mass and energy flow interactions through the boundaries and within the habitat space. Since the temperature and pressure in each zone are calculated at a single node, the lumped model entails well-distributed thermodynamic properties within the zone. However, this approach is still robust and has a low computational cost, so it has a strong advantage, enabling real-time simulation.

The mechanism by which mass and energy flow into and out of the control volume is shown in Fig. 5. Since the IE model is based on a lumped method to generate air temperature and pressure data with the given boundary conditions from other subsystems, a single node is used to represent a whole control volume. The temperature and pressure are calculated at the node, and it is assumed that the temperature and pressure are uniform in the control volume. The lumped system approach is a typical method to generate the simplest energy flow prediction model for buildings or any open system [41–43].

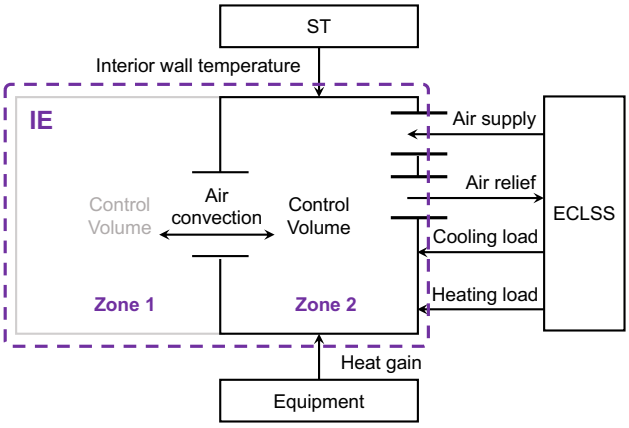

Fig. 5 A schematic of an open control volume system with boundary conditions.

The control volume approach is based on a set of governing equations which are used to capture the change in

mass, temperature, and pressure in the habitat. While detailed explanations of each term are provided in Ref.[40], the governing equations are briefly discussed in the following subsections.

1. Mass balance equation

The zero-dimensional conservation of the mass of dry air equation with a lumped method is described as follows.

$$\begin{aligned}\frac{\mathrm{d}m_{cv}}{\mathrm{d}t} &= \sum_i \dot{m}_i - \sum_e \dot{m}_e \\ &= \dot{m}_{sup} - \dot{m}_{rel} - \dot{m}_{leak} \pm \dot{m}_{conv}\end{aligned} \tag{1}$$

where m_{cv} is the mass of the air inside the control volume, $\dot{m}_i$ and $\dot{m}_e$ are the entering and exiting mass flow rate of the air crossing the boundary of the control volume, $\dot{m}_{sup}$ and $\dot{m}_{rel}$ are the mass flow rate of the supply and relief air by ECLSS, $\dot{m}_{leak}$ is the mass flow rate of the air leakage, and $\dot{m}_{conv}$ is the mass flow rate of the air convection between two control volumes.

2. Energy balance equation

The zero-dimensional conservation of energy equation for an open control volume system is described as follows.

$$\frac{\mathrm{d}E_{cv}}{\mathrm{d}t} = \dot{Q}_{cv} - \dot{W}_{cv} + \sum_i \dot{m}_i \left(h_i + \frac{v_i^2}{2} + g z_i \right) - \sum_e \dot{m}_e \left(h_e + \frac{v_e^2}{2} + g z_e \right) \tag{2}$$

where E_{cv} is the energy in the control volume, $\dot{Q}_{cv}$ is the heat transfer rate added to the control volume, $\dot{W}_{cv}$ is the rate of the boundary work done, h is the specific enthalpy of the air, v is the mean velocity of air, g is the gravitational acceleration, and z is the height at which mass transfer through the boundary occurs [44]. This base formulation can be further simplified by assuming the kinetic and potential energy and boundary work terms to be negligible. By implementing the given boundary conditions, the energy balance equation becomes the following equation.

$$\frac{\mathrm{d}U_{cv}}{\mathrm{d}t} = \dot{Q}_w + \dot{Q}_{ECLSS} + \sum_k \dot{Q}_{hg,k} + \dot{Q}_f + \dot{m}_{sup} h_t - (\dot{m}_{rel} + \dot{m}_{leak}) h_{cv} \pm \dot{m}_{conv} h_{conv} \tag{3}$$

where $\dot{Q}_w$ is the heat transfer rate of convection and radiation of the interior wall, $\dot{Q}_{ECLSS}$ is the thermal load by ECLSS, $\dot{Q}_{hg,j}$ is the heat gain, $\dot{Q}_f$ is the heat transfer rate from an internal fire, h_t is the specific enthalpy of air inside the air storage tank, h_{cv} is the specific enthalpy of air in the control volume, and h_{conv} is the specific enthalpy of air at the high pressurized zone. Subscript k indicates a subsystem that is either PW or ECLSS which generates heat from their equipment (e.g., compressor, fans, battery cells).

3. Coupled governing equations

A way to replace the explicit dependency of the IE model on tabulated (or experimentally determined) capacitance values and increase the model robustness is to directly couple temperature and pressure through the energy balance equation [43]. Maintaining the thermal and pressure interactions surrounding the air, or the zone in the context of the zonal modeling approach, the node representing the lumped air is replaced by a more elaborate formulation which takes into account the two-way coupling between temperature and pressure. It can be assumed that the volume of the interior habitat, which is practically confined by the wall of the ST, is constant. Additionally, air density can be expressed as a function of the specific enthalpy and pressure of the air, which are intensive thermodynamic properties according to the ideal gas assumption. Then, the left-hand-side term in each balance equation can be further derived by using the chain rule.

$$\frac{\mathrm{d}m_{cv}}{\mathrm{d}t} = V_{cv}\frac{\mathrm{d}\rho(h,P)}{\mathrm{d}t} = V_{cv}\left(\frac{\partial\rho}{\partial h}\right)_P\frac{\mathrm{d}h}{\mathrm{d}t} + V_{cv}\left(\frac{\partial\rho}{\partial P}\right)_h\frac{\mathrm{d}P}{\mathrm{d}t} \tag{4}$$

$$\begin{aligned}\frac{\mathrm{d}U_{cv}}{\mathrm{d}t} &= \frac{\mathrm{d}(m_{cv}u)}{\mathrm{d}t} = V_{cv}\frac{\mathrm{d}(\rho u)}{\mathrm{d}t} = V_{cv}\frac{\mathrm{d}(\rho h - P)}{\mathrm{d}t}\\ &= V_{cv}\left(\rho\frac{\partial h}{\partial t} + h\frac{\partial\rho}{\partial t} - \frac{\partial P}{\partial t}\right)\\ &= V_{cv}\left[\rho + h\left(\frac{\partial\rho}{\partial h}\right)_P\right]\frac{dh}{dt} + V_{cv}\left[h\left(\frac{\partial\rho}{\partial P}\right)_h - 1\right]\frac{dP}{dt}\end{aligned} \tag{5}$$

As explained above, the IE model can theoretically represent the multi-zonal deep space habitat. Each zone has a set of conservation of mass and energy equations. If there is more than one zone inside the habitat, the same number of sets of equations should be provided and connected to each other. The current IE model has two zones, and these zones are connected by a pocket door. By having two sets of balance equations, a system of equations for the two-zone model is derived below.

$$V_i\left(\frac{\partial\rho_i}{\partial h_i}\right)_{P_i}\frac{dh_i}{dt} + V_i\left(\frac{\partial\rho_i}{\partial P_i}\right)_{h_i}\frac{dP_i}{dt} = \dot{m}_{sup,i} - \dot{m}_{rel,i} - \dot{m}_{leak,i} + (-1)^{\mathcal{H}(P_i-P_j)}\,\dot{m}_{conv,i-j}, (i \neq j) \tag{6}$$

$$\begin{aligned}&V_i\left[\rho_i + h_i\left(\frac{\partial\rho_i}{\partial h_i}\right)_{P_i}\right]\frac{dh_i}{dt} + V_i\left[h_i\left(\frac{\partial\rho_i}{\partial P_i}\right)_{h_i} - 1\right]\frac{dP_i}{dt}\\ &\quad= \dot{Q}_{w,i} + \dot{Q}_{ECLSS,i} + \left(\sum_k \dot{Q}_{hg,k}\right)_i + \dot{Q}_{f,i} + \dot{m}_{sup,i}h_t - (\dot{m}_{rel,i} + \dot{m}_{leak,i})h_i\\ &\qquad+ (-1)^{\mathcal{H}(P_i-P_j)}\,\dot{m}_{conv,i-j}\left[\left(\mathcal{H}\left(P_i - P_j\right)h_{conv,i} + \left(1 - \mathcal{H}\left(P_i - P_j\right)\right)h_{conv,j}\right], (i \neq j)\end{aligned} \tag{7}$$

where subscripts $i, j \in \{1, 2\}$ represent a zone index. Balance equations can be rearranged by moving dt from the left-hand side to the right-hand side to make a system of equations. To simplify the equations, the right-hand-side terms

are replaced with b_i.

$$V_i \left(\frac{\partial \rho_i}{\partial h_i}\right)_{P_i} dh_i + V_i \left(\frac{\partial \rho_i}{\partial P_i}\right)_{h_i} dP_i = b_{COM,i} dt \tag{8}$$

$$V_i \left[\rho_i + h_i \left(\frac{\partial \rho_i}{\partial h_i}\right)_{P_i}\right] dh_i + V_i \left[h_i \left(\frac{\partial \rho_i}{\partial P_i}\right)_{h_i} - 1\right] dP_i = b_{COE,i} dt \tag{9}$$

Subsequently, the system of equations can be obtained as follows.

$$Ax = b \tag{10}$$

where

$$A = \begin{bmatrix} V_1 \left(\frac{\partial \rho_1}{\partial h_1}\right)_{P_1} & V_1 \left(\frac{\partial \rho_1}{\partial P_1}\right)_{h_1} & 0 & 0 \\ V_1 \left[\rho_1 + h_1 \left(\frac{\partial \rho_1}{\partial h_1}\right)_{P_1}\right] & V_1 \left[h_1 \left(\frac{\partial \rho_1}{\partial P_1}\right)_{h_1} - 1\right] & 0 & 0 \\ 0 & 0 & V_2 \left(\frac{\partial \rho_2}{\partial h_2}\right)_{P_2} & V_2 \left(\frac{\partial \rho_1}{\partial P_2}\right)_{h_2} \\ 0 & 0 & V_2 \left[\rho_2 + h_2 \left(\frac{\partial \rho_2}{\partial h_2}\right)_{P_2}\right] & V_2 \left[h_2 \left(\frac{\partial \rho_2}{\partial P_2}\right)_{h_2} - 1\right] \end{bmatrix}$$

$$x = \begin{bmatrix} dh_1 & dP_1 & dh_2 & dP_2 \end{bmatrix}^T$$

$$b = \begin{bmatrix} b_{COM,1} & b_{COE,1} & b_{COM,2} & b_{COE,2} \end{bmatrix}^T dt$$

In every sampling time, this linear system of equations is solved to get the updated current solutions below.

$$\begin{aligned} h_i^{n+1} &= h_i^n + dh_i \\ P_i^{n+1} &= P_i^n + dP_i \end{aligned} \tag{11}$$

where subscripts, $n+1$ and n, indicate the time step. Additionally, the air temperature in each zone can be calculated with the specific enthalpy of the air in the corresponding zone. As the IE model uses the ideal gas assumption and constant specific heat of air, the air temperature formula can be derived below.

$$T_i^{n+1} = \frac{h_i^{n+1}}{c_p} \tag{12}$$

C. Module 2: ECLSS

ECLSS provides the necessary measures to ensure the survival and well-being of crew members in a deep space habitat. It is the interconnected system that processes cabin air, wasted water, and solid waste, as well as providing

control actions to maintain temperature, pressure, oxygen level, and others related to the well-being of crew and equipment. It also ensures that suitable conditions are maintained for the structure, subsystems, equipment, and samples of scientific research in the absence of a crew. In HabSim, the ECLSS module includes two control systems, an Active Thermal Control System (ATCS) and an Interior Pressure Control System (IPCS), which are responsible for maintaining the interior temperature and pressure of the habitat, respectively. As these two control systems are physically separated systems, as shown in Fig. 6, components of one control system do not interact directly with those of the other control system. By the inputs made by users, the initial conditions and the design parameters of ECLSS are established. The ECLSS exchanges signals, which can be either cyber information such as sensor readings or physical information such as mass flow rate and heat transfer rate, with other subsystems with the help of the CB. Interactions of the ELCSS with the lunar environment or disturbances such as dust accumulation and meteorite impacts are triggered by the signals from the DB.

In this section, the overall model architectures will be provided along with the governing equations for each component. More detailed explanations of terms and derivations of them are provided in Ref. [45].

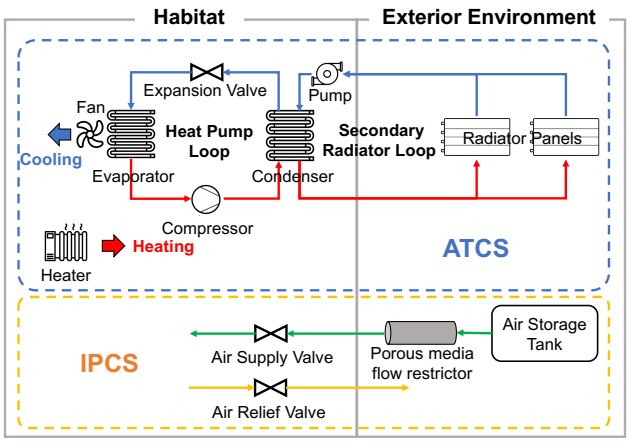

Fig. 6 Schematic of the ATCS and IPCS in the ECLSS.

1. Active thermal control system

The ATCS provides space conditioning to the interior environment of the habitat. As a cooling system, a vapor compression heat pump connected to a secondary radiator loop has been suggested as the most feasible option to actively control the thermal environment of a lunar habitat [45–47]. Employing a heat pump not only leads to a notable decrease in the required size of radiators for heat dissipation, but also decreases environmental vulnerabilities such as fluctuations in surface temperature and accumulation of dust. This integration can guarantee continuous heat rejection to the exterior environment regardless of the heat sink temperature.

A four-component vapor compression refrigeration cycle SR: the cycle is used only for cooling. Should we use "vapor

compression cycle" or "vapor compressionr refrigeration cycle"? (i.e., an evaporator, a compressor, a condenser, and an expansion valve) is a system widely utilized for cooling in various Earth applications due to its energy efficiency. In HabSim, each component has been developed with the corresponding governing equations. First, a positive displacement compressor model is used to drive the dynamical behaviors of the system by producing the refrigerant mass flow. It is the main component that consumes electrical power in the cooling system. Second, a quasi-stead expansion valve is developed based on the orifice equation. Next, two heat exchangers, a condenser and an evaporator, are modeled as a two-phase heat transfer process based on the lumped approach. Transient mass and energy balance equations are used along with the number of transfer units (NTU) method to compute heat and mass transfer, as well as the phase change of the refrigerant. Additionally, various assumptions are implemented to enable real-time intermediate fidelity computation including neglecting pressure drop, zero subcool and zero superheat, and isenthalpic expansion process. Detailed explanations of the equations and terms are provided in [45].

The radiator system comprises multiple radiator panels, each equipped with an internal tube to facilitate heat exchange between the radiator plate and the fluid circulating through the tubes. This fluid carries heat from the condenser in the heat pump loop and disperses it to the radiator panels, where it is emitted through radiation. The radiator panels are modeled using the quasi-steady energy balance equation, while the energy balance on the heat transfer fluid in the tubes is developed using a transient partial differential equation. Although the secondary radiator loop system is not always explicitly categorized as part of ECLSS, it is discussed due to its close connection and importance in regulating habitat thermal conditions and potential fault impacts [40].

- A quasi-steady energy balance for the radiator surface:

$$\frac{T_f - T_r}{\frac{l}{\pi r}\frac{1}{U_f} + \frac{\delta}{\lambda_d}\gamma + \frac{w}{\lambda_r \eta_r}} = \epsilon_m \sigma {T_r}^4 - \alpha_m G_s sin(\theta(t)) \tag{13}$$

where T_f denotes the local fluid temperature, T_r stands for the local radiator surface temperature for long-wave radiation, r indicates radius of the tube, U_f denotes the convective heat transfer coefficient in the tube, δ denotes the thickness of the dust layer, which adds an extra thermal resistance, γ stands for the area fraction of dust cover, w stands for the half thickness of the radiator fin, η_r represents the efficiency of the fin, λ indicates the thermal conductivity with subscripts d and r denoting the dust and radiator fin, respectively, ε_m and α_m denote the emissivity and the absorptivity of the radiator surface with dust contamination, σ stands for the Stefan-Boltzmann constant, G_s is the direct normal solar radiation (assumed to be the lunar solar constant), and $sin(\theta(t))$ takes into account the daily solar input variation.

- A transient energy balance on the heat transfer fluid in the tube:

$$\rho_f c_{p,f} \pi r^2 \left(\frac{\partial T}{\partial t} + v_f \frac{\partial T_f}{\partial z} \right) = \frac{T_r - T_f}{\frac{1}{2\pi r U_f} + \frac{1}{2l}\left(\frac{\delta}{\lambda_d}\gamma + \frac{w}{\lambda_r \eta_r}\right)} \tag{14}$$

  where ρ_f is density, $c_{p,f}$ is specific heat, v_f denotes the velocity of the heat transfer fluid, l stands for the extended length of the radiator fin. The subscript f denotes the heat transfer fluid in the radiator loop.

Detailed explanations of the equations, terms, and correlation equations are provided in Ref. [45]. It is important to note that the ATCS described in this paper is tailored for a lunar habitat, taking into account the specific lunar environment and material properties such as lunar dust and solar irradiation. Users are allowed to modify these values according to their research purposes and the applications under study.

It is assumed that lunar habitats will have thick walls for thermal insulation along with protection from radiation and physical impacts, such as micrometeorite impacts and moonquakes. Hence, there will be limited heat exchange with the exterior environment, which minimizes heat loss in the habitat [45]. The internal heat loads of the habitat include the electricity consumed within the habitat that is dissipated as heat transfer, as well as the metabolic release from the crew. Therefore, normally only cooling will be necessary to reject the waste heat generated from the interior sources. However, heating is still required under certain scenarios (e.g., damage to the habitat protection wall) and mostly during the cold lunar night. Due to the very low heat sink temperature in the lunar night environment, utilizing a heat pump system for heating is not feasible, making an electric resistance heater a more viable choice. Therefore, an ideal heater model with 100 % efficiency is used as a heating system in the ATCS, as illustrated in Fig. 6. The heater is controlled by an off-off controller that feeds the air temperature of each zone in the habitat with the deadbands, which adjusts the heating load to maintain the temperature of each zone individually to the setpoint temperature defined by the users.

2. Interior pressure control system

The IPCS maintains the interior pressure in each zone of the habitat, respectively, at the desired level according to the requirements of specific mission periods, such as manned and unmanned periods. The IPCS consists of an air supply line connected to an air storage tank and an emergency air relief valve, as depicted in Fig. 6. It is assumed that the time delay in valve opening is negligible. Therefore, the dynamical opening or closing of a valve is not modeled, and instead a quasi-steady valve model, which treats the flow of air to be at steady-state at each time step, is implemented. The reference values used to size the storage tank, the flow restrictor, and the valves are based on the data in Ref. [48] for the respective components used on the ISS. The dimensions of the components can be further adjusted by user input. The size of the components is determined considering the severity of the potential leakage. If there is a large leak beyond the compensating capacity of the IPCS, the indoor air pressure will be out of control and the habitat will be in an extremely dangerous situation that requires immediate intervention action from the AG.

The IPCS in HabSim includes models for an air storage tank, isolation valves with on/off logic control, and a flow restrictor which restricts the air flow rate. Since pressure is almost uniform inside each zone while the pocket door is closed, the interior atmosphere of the habitat is considered to show a uniform pressure distribution at each zone. These lumped pressures are to be controlled by the IPCS, respectively. The main assumption of the IPCS model is that the pressure loss caused by friction in the air transport line is negligible.

The air storage tank is modeled as a single control volume. The lunar surface temperature varies from −180 °C to 124 °C [49]. A storage tank could be inside the habitat itself or left outside with a regolith layer to reduce the impact of the ambient temperature of the space on the tank. Insulation of the tank is important to minimize thermal fatigue on the material and prevent earlier failure of a tank. In the model, it is assumed that the storage tank is perfectly insulated, and the air temperature inside the storage tank is constant. With this in mind, a mean temperature of 0 °C is assumed to be constant inside the tank. The particular choice of temperature value is not critical to the functionality of the IPCS. The temperature variation of the air stored in the tank as a result of a change in pressure is negligible, as the mass withdrawn is relatively small compared to the remaining air inside the tank. Based on these assumptions and features, a simple mass balance equation for the storage tank can be written.

$$\frac{d\left(\rho_{st} V_{st}\right)}{dt} = V_{st} \frac{d\rho_{st}}{dP_{st}} \frac{dP_{st}}{dt} = -\dot{m}_{sup} \tag{15}$$

where the subscript st denotes the storage tank, ρ is density, V is the volume, P is the pressure, and $\dot{m}_{sup}$ indicates the mass flow rate of air supplied to the habitat interior.

A quasi-steady model is used to describe the mass flow rate that flows through the valve. The dynamics of the valve during opening and closing is not included as it is assumed that the time delay for a valve to open is negligible compared to the duration of the valve opening. The model is represented as follows.

$$\dot{m}_v = \rho_{air} K_v \sqrt{\Delta P_v} \tag{16}$$

where $\dot{m}_v$ is mass flow rate at the valve, K_v is the valve flow coefficient, often given by the manufacturer from empirical data, ΔP_v is the pressure drop across the valve, and ρ_{air} is the air density. The valves are operated by actuators that determine the cross-sectional area of the flow passage. A controller is implemented to send signals to the valve actuators depending on the difference between the current pressure value in the interior habitat and the setpoint pressure determined by the users.

The air supplied from a storage tank goes through a flow restrictor before entering the IE to limit the maximum flow rate. The restrictor is modeled with a porous media approach. A simple 1D flow model with no thermal effects is

considered. According to Darcy's law, the mass flow rate going through the restrictor is expressed as follows.

$$\dot{m}_{sup} = \rho_{air} A \frac{k_m}{\mu_{air}} \frac{(P_v - P_{int})}{l} \tag{17}$$

where A and l are the cross-sectional area and length of the flow restrictor respectively, k_m is the media permeability, μ_{air} is the dynamical viscosity of air, P_v is the supplied air pressure after the isolation valve that is linked to the air storage tank, and P_{int} is the habitat interior pressure.

3. ECLSS damageable components

Currently, ECLSS has nine damageable components due to the disruptive events designed in HabSim: Radiator panel clearance, radiator panel paint conditions, evaporator, condenser, fan, heater, and compressor in ATCS, and air storage tank and valves in IPCS. Depending on the scenario case, location and intensity level (IL) of the disturbances, various components can be damaged with different severity. Furthermore, the nine damageable components can be divided into two categories: located in the exterior environment or in the interior environment. For instance, if a micrometeorite impact hits the radiator panels, which are located in the exterior environment, dust accumulation and paint degradation of the panels occur, while the other components placed in the habitat are not affected. Similarly, if the impact penetrates the structural layers of the habitat and hits the ECLSS directly, it leads to damage to the evaporator, condenser, fan, heater, compressor, air tank, and valves, which are components in the interior environment, whereas the radiator panels are not.

Initial damages resulting from disruptive events are hypothetically predetermined. For instance, a micrometeorite impact with an IL at four could harm the compressor in the habitat. This initial damage would result in a decrease in compressor performance, translating into a 40% reduction in the mass flow rate of the refrigerant, even when the compressor power consumption remains constant. The IL associated with each disruptive event range from one to five; where one indicates zero damage, while five represents the most severe case. Each IL has the potential to induce specific initial damage to the habitat. For example, ILs of four and five micrometeorite impact scenarios can breach the SPL and ST layers, causing air leakage at varying rates due to differences in the penetration radius. In contrast, ILs of two and three result only in heat generation in the SPL and ST layers due to the impact, along with a reduction in the thickness of the lunar regolith layer. In the case of an internal fire scenario initiated due to flammable materials or equipment, the initial fire radius and spread rates differ based on the IL. Despite the initial damages being grounded in hypothetical assumptions, the simulation model is constructed using principles of physics, where component models are interconnected with other relevant component models. This integration enables HabSim simulation results to include cascading effects based on physics. Details of disturbance scenarios and corresponding damage cases in ECLSS components are provided in Ref. [21, 40].

III. Performance-based Resilience Assessment

RETHi has developed a resilience-oriented habitat design process [50]. This process begins by identifying design requirements at the habitat-, subsystem-, and component-level through functional hazard analysis, state-trigger analysis, and safety control evaluation (referred to as top-down requirements development). Subsequently, a preliminary design of a deep space habitat is created based on these identified requirements. The preliminary design is then assessed in reverse order, starting from the component-level, subsystem-level, and finally the habitat-level (referred to as bottom-up design verification), through comparison of safety controls and evaluation of the system resilience. HabSim is designed to facilitate the habitat design phase. It is capable of producing state variable data sets at the various levels to compare the effectiveness of habitat design and safety controls in terms of system resilience. This section will delve into the performance-based resilience assessment, which constitutes the second part of the proposed framework shown in Fig. 2, and also serves as the final step of the habitat design process.

A. Performance curves

The first step in assessing the resilience of a system involves developing performance curves using various state variables generated by HabSim. For instance, the performance state of a heater (component-level) can be identified by assessing the heating load in relation to the designed capability, whereas the performance state of IPCS (subsystem-level) can be evaluated based on the air supply rate and the amount of air stored in tanks. Furthermore, the performance state at the habitat-level can be determined by the indoor air temperature or pressure.

Fig. 7 Severity ranges of a state variable.

The state variables generated by HabSim are expressed in their unique unit and order magnitude, posing a challenge when attempting to compare one value against another. For example, indoor air temperature and pressure behaviors cannot be directly compared to each other due to their different units and order magnitude. To overcome this challenge and ensure generality, the performance state should be further assessed by normalizing the corresponding state variable [51]. Moreover, it is essential to take into account the severity of the value of the state when constructing performance curves [52]. There are three possible severity ranges of the state: acceptable, warning, and hazardous ranges, as illustrated in Fig. 7. In Fig. 7, SV represents the state variable, SV^* denotes the desired state value, $SV^{*\pm}$ indicates the upper and lower limits of the acceptable range, respectively, and $SV^{*\pm\pm}$ represents the upper and lower thresholds of the warning range, respectively. For example, if the indoor air temperature remains close to the preferred level, even exhibiting some oscillatory behavior but staying within an acceptable range, it should not be considered as a performance loss. Furthermore, the evaluated performance curve should be able to reflect the severity of the hazardous range more

than the warning range. For this reason, different values of a weight factor are incorporated into the performance metric. Consequently, the performance state, PS, can be mathematically defined as follows.

$$\begin{aligned} PS\left(t\right) &= \max\left(0, 1 - w_{\mathrm{r}} PS_{\mathrm{loss}}\right) \\ &= \max\left(0, 1 - w_{\mathrm{r}}\left[\mathcal{H}\left(SV^{*^{-}} - SV\left(t\right)\right)\left|\frac{SV^{*^{-}} - SV\left(t\right)}{SV^{*^{-}} - SV^{*^{--}}}\right| + \mathcal{H}\left(SV\left(t\right) - SV^{*^{+}}\right)\left|\frac{SV\left(t\right) - SV^{*^{+}}}{SV^{*^{++}} - SV^{*^{+}}}\right|\right]\right) \end{aligned} \tag{18}$$

It should be noted that the calculated performance state PS is a dimensionless value due to normalization. w_{r} denotes the weight factor indicating the severity of a state variable, which is defined as follows.

$$w_{\mathrm{r}}\left(t\right) = \begin{cases} 0 & \text{if } SV\left(t\right) \in \text{Acceptable range} \\ 0.5 & \text{if } SV\left(t\right) \in \text{Warning range} \\ 1 & \text{if } SV\left(t\right) \in \text{Hazardous range} \end{cases} \tag{19}$$

Decision-makers can adjust the values of 0.5 and 1 of w_{r} in the warning and hazardous ranges, respectively.

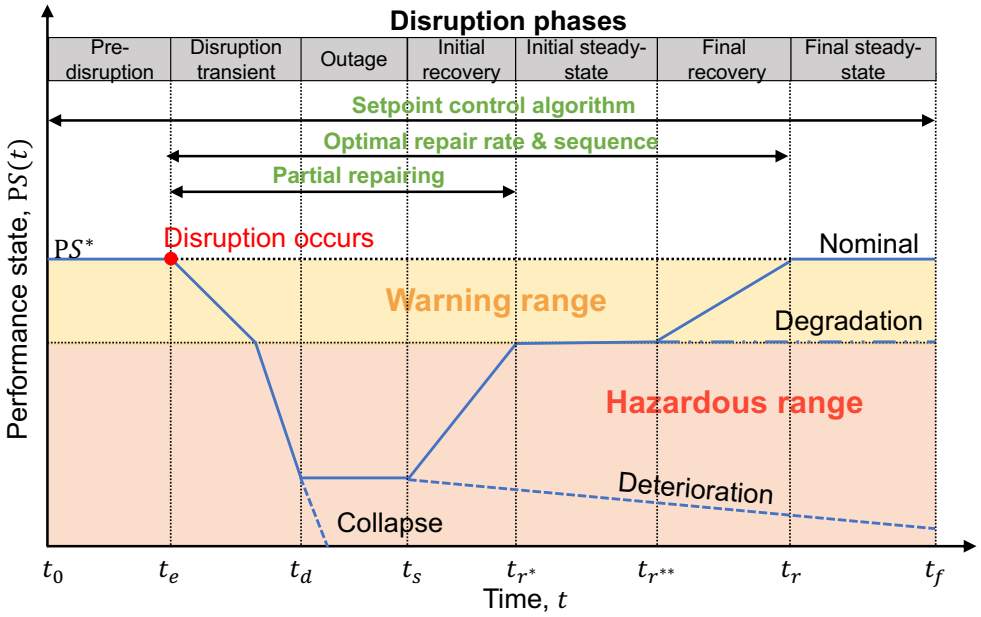

Fig. 8 Conceptual performance curve with disruption phases and potential operating strategies.

Fig. 8 illustrates a conceptual example of a performance curve. In addition, it describes seven potential disruption phases defined based on the behavior of the performance curve [53, 54]. Starting with the initial time, t_0, the system is in the pre-disruptions phase until a disruption occurs at t_e. Once the performance reduction stops at t_d, it enters the disruption transient phase. Performance remains at a minimum level during the outage phase until it starts to recover at t_s. During the initial recovery phase, the performance gradually returns to the lower saturation level of the warning

range, continuing until t_{r^*}, at which point it enters the initial steady-state phase. Performance remains in this state until the damage is repaired again, which occurs at $t_{r^{**}}$. t_r is the time at which the performance is finished recovering and can be at or below the initial state value. By analyzing the performance curve, the status of the system can be evaluated. For instance, the minimum value of a performance state is zero, while the maximum value is one, which is the nominal performance PS^*. If the performance state continuously decreases after the disruption, it indicates a system collapse. Additionally, a value below one represents performance degradation or deterioration, depending on the presence or absence of a recovery phase after the outage phase. In addition, applicable operational strategies and the appropriate period for each are indicated in Fig. 8. These strategies are further discussed in the following section.

B. Quantification metrics

To evaluate the resilience of a system, it is crucial to carefully choose the resilience quantification metrics that correspond to its distinct characteristics and specific requirements. For example, a compressor in ATCS that is physically connected to different components such as heat exchangers and an expansion valve through a pipeline, making replacement a challenging task. Thus, it is more practical for the compressor to be designed to endure and absorb damage effectively with minimal initial performance loss, rather than focusing on quick repair or replacement. In contrast, a fan in the ATCS can be easily swapped with a spare unit in the event of damage, highlighting the importance of designing the ATCS system for easy fan replacement. Examining from the perspective of the subsystem, the repair of a damaged ATCS system can be laborious and intricate, involving various procedures such as draining, vacuuming, fixing, conducting refrigerant leak assessments, recharging with refrigerant, and carrying out unit tests. Therefore, a resilient design for the ATCS system is vital to ensure its continuous operation even with reduced performance due to damage. On the contrary, the primary goal of IPCS, which is responsible for regulating the indoor air pressure to the desired level, is crucial for the survival of the crew. Hence, it should be designed for immediate repair, as any minor performance loss may not be tolerable. At the habitat level, a certain degree of performance loss over an extended period could be acceptable. However, it is vital to avoid significant initial performance loss in the habitat, since it could trigger a chain of cascading impacts on the entire subsystem, potentially resulting in system failure.

Researchers in various scientific and engineering fields have developed numerous resilience quantification metrics [27–29, 31–35, 37, 55, 56]. Resilience metrics based on a single-index were developed to cover a particular dimension of system resilience, such as initial performance loss, recovery duration, total or averaged performance loss, and final performance status, whereas multi-index metrics combine different single-index metrics to assess the overall resilience of a system [54]. This paper deploys two fundamental single-index metrics as preliminary known methods. It is important to highlight that the use of sophisticated multi-index quantification metrics can improve the comprehensive assessment of complex SoSs.

1. Recovery duration resilience

This metric measures the recovery time it takes for the system to return to or above its nominal performance state [27, 32, 55, 56]. It is important to note that the results do not reflect the severity of the disruption or the total performance loss of the system. Additionally, the measured value of this metric is expressed in units of time.

$$\mathcal{R}_{\mathrm{r}} = t_r - t_e \tag{20}$$

2. Resilience loss

Resilience loss measures the total performance loss during the investigation time [27, 29, 31, 35, 37, 54–56]. This metric calculates the area between the nominal performance and the true performance under damage. The metric is defined as follows.

$$\mathcal{R}_{\mathrm{loss}} = \int_0^{t_f} PS^* - PS\,(t)\,dt \tag{21}$$

It should be noted that the value of resilience loss is in units of time since it integrates dimensionless performance state in time.

C. Potential resilience improvement methods

Resilience of deep space habitats can be achieved through two primary approaches [38]. The first method involves appropriately designing the system architecture, which includes over-designing, incorporating spare equipment, and sophisticated system configurations. For example, the ATCS can effectively absorb damage by over-sizing its system capacities. By having large capacities that exceed nominal operation requirements, the system can adequately regulate habitat conditions even with reduced performance. Incorporating spare equipment into the system is another way to improve its restorability. For instance, by adding a spare heat exchanger that remains inactive during normal conditions but can be activated when the primary one is damaged, the overall performance of the ATCS can be quickly restored, while it also secures enough time to repair or replace the damaged component. It is important to highlight that the first method can make a system resilient against disturbances with a certain degree of severity; disturbances with an exceeding severity that a system cannot manage can still result in a system failure. To overcome this insufficiency of the first method, repair and recovery actions must be integrated into the design of habitats. Thus, the second category for enhancing resilience is the optimization of operating strategies. This approach involves actively controlling setpoints, optimizing repair rates or sequences, and partially repairing damaged components. For example, if components of the ATCS are damaged, it may take longer to achieve the desired indoor temperature. In such cases, adjusting the setpoint temperature beyond the desired level can help the ATCS regulate the indoor temperature reaching the required level faster by increasing its workload. Another example is to prioritize the repair action of multiple damaged components in

the order of importance to quickly restore the system performance to normal conditions. If there are multiple available repair actions with different rates, strategically assigning these actions can accelerate recovery. Lastly, it is appropriate to repair damaged components only to a certain level that they can function adequately, rather than perfectly, before moving on to other damaged components to restore overall system performance to an acceptable level. Fig. 8 illustrates the suitable disruption phase for each operational strategy.

This paper aims to optimize one of the operating strategies, specifically the repair sequence of damaged ECLSS components, using habitat-level data such as indoor air temperature and pressure. To achieve this, performance curves for indoor air temperature and pressure are developed to assess the habitat's resilience using specific metrics. The detailed steps for each process are discussed in the following section along with an illustrative case study.

IV. An Illustrative Case Study

In this section, an illustrative case study will be provided to showcase the proposed framework and demonstrate its capabilities. A disruptive scenario case, specifically a micrometeorite impact scenario with an IL at five, will be used to generate habitat performance reduction. The results will be compared with those under nominal conditions. In the micrometeorite impact scenario, six different repair sequence strategies of damaged ECLSS components are implemented to present different behaviors of the system. Based on these outcomes, performance curves are generated to assess the resilience of the system with different repair sequences. Comparison of evaluated resilience values will provide the optimal repair sequence strategy to quickly recover the habitat.

A. Key performances and requirements

HabSim can generate various state variable data from the component-level to the habitat-level. As a component-level variable state, the model can provide the air flow rate by the ATCS, the power consumption of a cooling fan, the interior wall surface temperature, among others. The ECLSS total power consumption, the cooling load by ATCS, the level of power availability, and the total power generation rate of solar PV and nuclear generators can be categorized as the state variable at the subsystem level. Lastly, the interior air temperature and pressure and the overall power consumption by all subsystems can be considered as the state variable at the habitat-level. The goal of this illustrative case study presented in this paper is to evaluate the performance of the habitat at the habitat-level to optimize a repair sequence of damaged ECLSS components. Therefore, IE air temperature and pressure are mainly used to assess the system.

Scenarios can be divided into unmanned and manned mission periods. During unmanned missions, it is assumed that there is no crew present inside the habitat and that the habitat functions autonomously following predetermined schedules or remote control from the ground on Earth. During this phase, the necessary habitat conditions are established primarily with a focus on ensuring the safety of electronic equipment and scientific research samples. In manned scenarios, the crew will reside in the habitat and can actively operate and supervise the habitat system. Since the main objective of the

habitat is to serve as a secure and habitable shelter for the crew, the required conditions should be planned based on ensuring the crew's safety. Therefore, the acceptable, warning, and hazard ranges for each mission period are defined based on the ECLSS standards [57], along with the relevant literature on human well-being conditions and recommended operational parameters for electronic equipment [58, 59]. A summary of the IE conditions is described in Table 2.

Table 2 Indoor temperature and pressure criteria for different mission periods.

	Pressure (kPa)					Temperature ($^{\circ}C$)				
Mission Period	P^{*--}	P^{*-}	P^{*}	P^{*+}	P^{*++}	T^{*--}	T^{*-}	T^{*}	T^{*+}	T^{*++}
Unmanned	10	65	101	102	500	4	4	25	80	80
Manned	37	70	101	102	500	4	20	25	27	51

B. Nominal operating conditions

During nominal conditions, lunar habitats are still exposed to harsh environmental conditions including intense solar radiation and extremely fluctuating lunar surface temperature [49]. Furthermore, a lunar day is about 29 Earth days, so habitats are exposed to extremely hot or cold surface temperatures for a long time. Therefore, it is necessary to simulate and explore two nominal operating conditions to investigate habitat performance: a lunar day and a lunar night. In this case study, these two subcases are represented by imposing different interior wall surface temperatures; the constant surface temperature at 30 °C for a lunar day and at 20 °C for a lunar night. It is assumed that the pocket door remains closed throughout the simulation period to observe how ECLSS can control each zone separately. Moreover, the initial indoor temperatures vary, with one zone at 26 °C and the other at 24 °C, whereas the initial indoor pressures are the same at 101.3 kPa for both zones. Habitat performances during lunar day and night periods are illustrated in Fig. 9 and 10, respectively.

During a lunar day, a rise in indoor air temperature is observed due to the high temperature of the interior wall surface, which is at 30 °C, as illustrated in Fig. 9. Once the temperature surpasses the upper dead band set at 26 °C, the ECLSS initiates the temperature regulation until it decreases to 24 °C. The indoor pressure correlates with the temperature due to the two-way coupling of temperature and pressure. The cooling system comprises two adjustable elements: a compressor and fans, each dedicated to a zone. Furthermore, it operates as a Variable Air Volume (VAV) system that manages multiple zones by controlling air flows through a single heat pump loop. This cooling system design gradually minimizes the temperature variation between zones, even when the simulation starts with distinct initial temperature conditions for each zone. While indoor air temperatures converge, indoor air pressures act independently. This is because there is no air mass flow to or from the zones, indicating closed control volumes and thus maintaining independent behaviors. The average cooling load upon activation is approximately 4 kW, with a total power consumption rate of approximately 1.2 kW. These results yield a coefficient of performance (COP) of approximately 4.2, which is a typical value for heat pump systems.

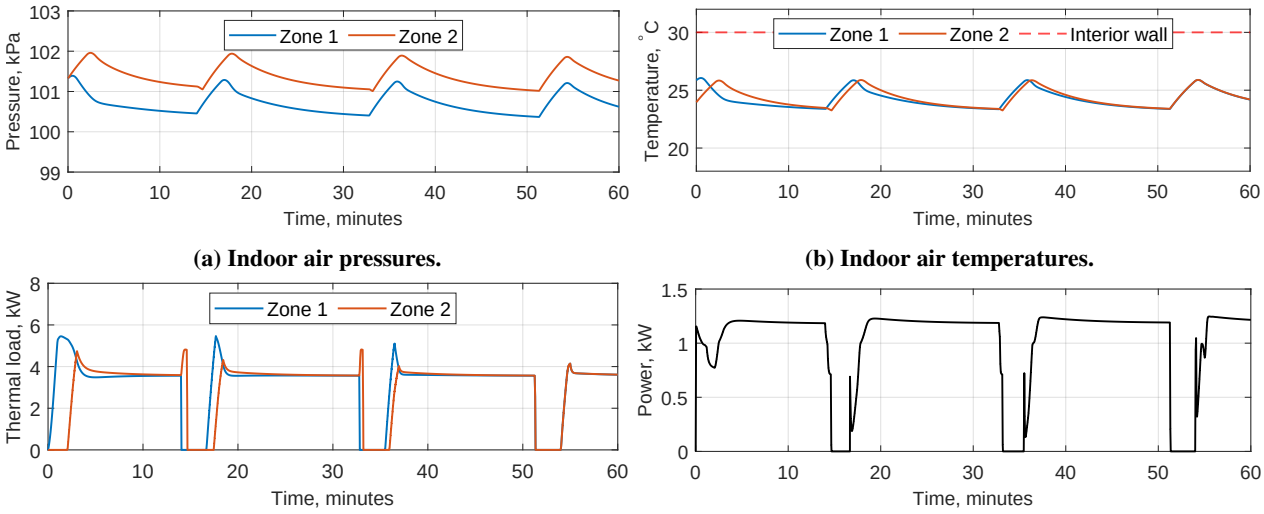

(a) Indoor air pressures.

(b) Indoor air temperatures.

(c) Cooling load by ECLSS.

(d) Total power consumption rate by ECLSS.

Fig. 9 Habitat behaviors (state variables) during a lunar day.

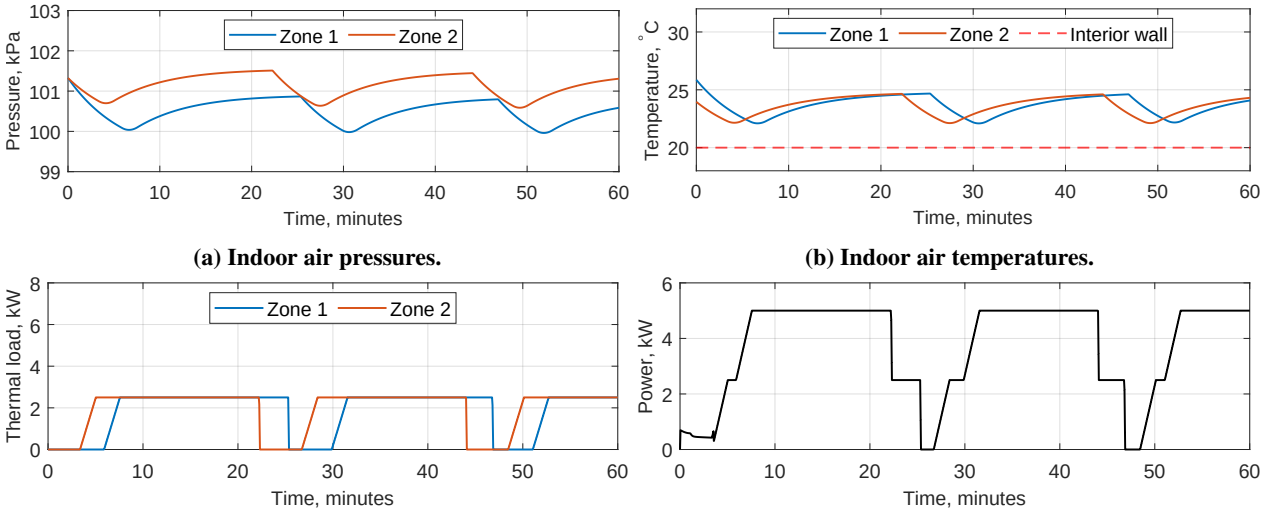

(a) Indoor air pressures.

(b) Indoor air temperatures.

(c) Heating load by ECLSS.

(d) Total power consumption rate by ECLSS.

Fig. 10 Habitat behaviors (state variables) during a lunar day.

Fig. 10 illustrates habitat performances during a lunar night, where the initial temperature and pressure conditions are the same as those employed for simulating a lunar day, but with modified boundary conditions. In this case, the interior wall surface temperature is set to 20 °C, leading to a decrease in temperature. To compensate for this drop, a heater with a capacity of 2.5 kW is installed in each zone. In contrast to the cooling system, which comprises two adjustable components, the two heaters function as independent components, resulting in a continuous temperature differential between two zones. As the heaters are assumed to operate with 100 % efficiency, the maximum power consumption rate of the heating system is 5 kW.

C. A micrometeorite impact scenario

One of the primary disruption scenarios hypothetically designed in HabSim is a micrometeorite impact. Users have the flexibility to select several key parameters, including the IL of the impact, its location, and the time at which it occurs. Impacts with IL at four or five, representing two extreme cases, are designed to penetrate the SPL and ST, directly hitting systems within the habitat depending on the impact location. The radius of penetration is determined depending on the IL and is assumed to remain constant over time until the AG repairs it. The air leak flow rate resulting in penetration is determined by both the radius of the hole and the difference between the current interior pressure and the constant exterior pressure. This air leak causes a rapid drop in the indoor air pressure along with the interior air temperature as they are coupled.

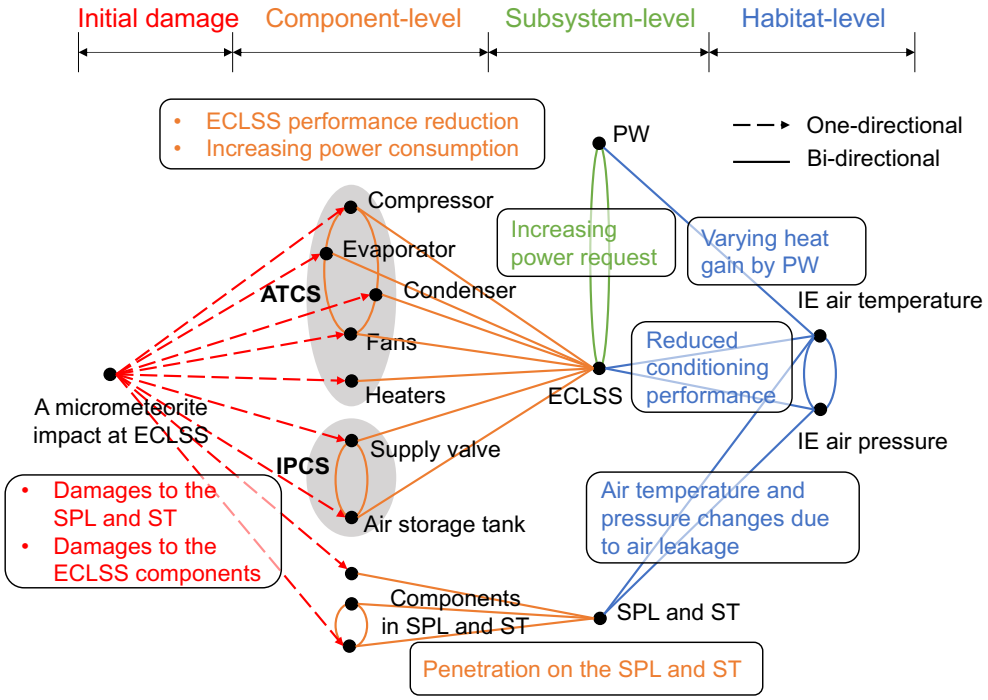

Fig. 11 Damage propagation and cascading effects due to a micrometeorite impact at ECLSS.

The ECLSS in HabSim has seven damageable components in the habitat, which are modeled to experience performance degradation to a specific degree depending on the IL of the disruption. The impact can have different types of performance reduction effect on each component. In Ref. [40], detailed explanation of the effects of initial damage is provided. The effect can propagate to other components, subsystems and, eventually, the habitat's performance based on physics-laws; a faulty compressor, for instance, will result in a decrease in the flow rate of the refrigerant while consuming the same amount of power. The damage propagation triggered by the initial damage from the impact is illustrated in Fig. 11.

In this case study, the optimal sequence is investigated to repair damaged ECLSS components, which are divided

into three categories: cooling systems, heating systems, and IPCS. To determine the repair sequence of the components within each category, simulations are performed to assess the impact of each component on the corresponding system performance, as shown in Fig. 12. Notably, the heating system consists only of an electric resistance heater, thus our focus shifts primarily to the cooling system and IPCS. The evaluation involves experiments under predetermined conditions: a starting indoor air temperature of 35 °C for the cooling system and an initial indoor air pressure of 100.3 kPa for the IPCS. In these tests, each component is individually subjected to a uniform performance reduction and the efficiency of the system is assessed based on its ability to regulate indoor air temperature and pressure. The results dictate that the cooling system should be repaired in the sequence of compressor, fan, evaporator, and condenser, while the IPCS repair should follow the order of air supply valve and then storage tank, optimizing the efficient restoration of system functionality. Based on these predefined orders, six combinations of repair sequences, consisting of cooling and heating systems, and IPCS, will be explored.

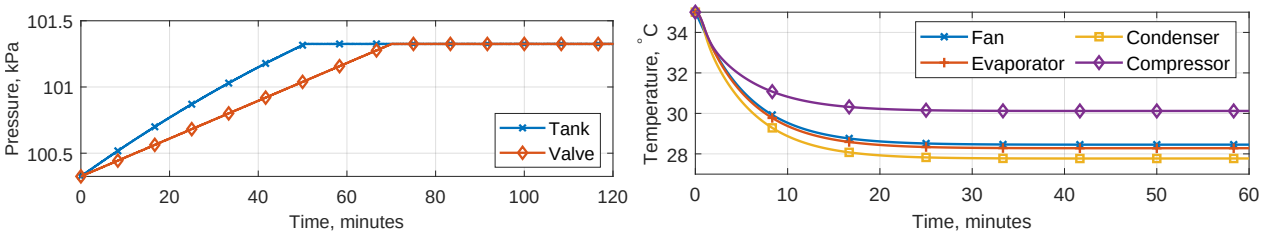

(a) Variations in indoor air pressure behaviors. **(b) Variations in indoor air temperature behaviors.**

Fig. 12 Comparative analysis depicting the importance of each component.

To understand the effect of the micrometeorite impact on the habitat, it is important to investigate the response of the habitat in the absence of any repair actions. For the purposes of this study, the IE air temperature and pressure are mainly discussed. The micrometeorite impact is assumed to occur 10 minutes after the simulation begins, with an IL at five, indicating the most extreme case. The impact with IL at five is designed to create a penetration in the SPL and ST with a radius of 7 cm. The AG is called immediately after impact and completely repairs the penetration at 14 minutes. Before the impact occurs, the interior air temperature and pressure are regulated by ATCS and IPCS in ECLSS at 25 °C and 101.3 kPa, respectively. When the impact occurs, the air temperature and pressure drop rapidly due to air leakage and the corresponding loss of mass and heat from the interior to the exterior, as illustrated in Fig. 13. The indoor air pressure decreases until the AG fully repairs the penetration. Then, it gradually increases due to the increase in temperature and the air supply by the IPCS. Once indoor air temperature stops increasing, the pressure increase rate is much slower due to damaged components in IPCS. Similarly, the indoor temperature decreases right after the impact, but increases even before the penetration is fixed, and returns to around the ATCS setpoint temperature. This is because after losing air pressure, the air capacity within the habitat is so low that the small heating load from damaged ATCS can quickly change the air temperature [40]. Therefore, despite the reduced performance of the heating system, the air

temperature returns to its nominal conditions, which is not a truly healthy condition.

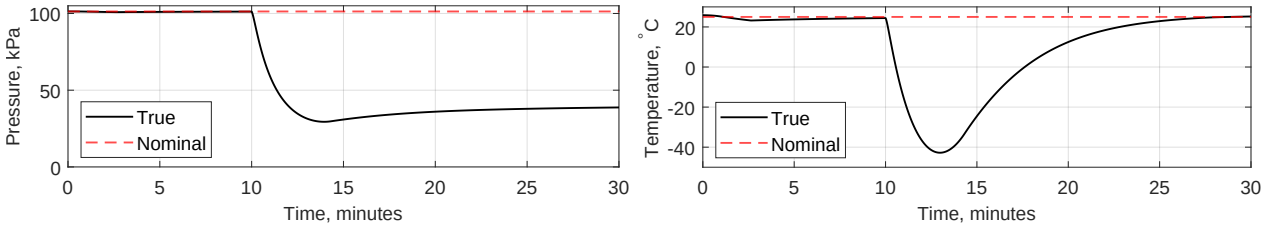

(a) Indoor air pressures. **(b) Indoor air temperatures.**

Fig. 13 Habitat behaviors (state variables) under a micrometeorite impact scenario.

D. Resilience assessment

To evaluate and identify an optimal repair sequence strategy, indoor air temperature and pressure behaviors are generated with six different repair sequences for damaged components of ECLSS, as illustrated in Fig. 14. The simulation results indicate that the AG completes the repair of the hole caused by the impact at 15 minutes. It resumes the repair action for damaged ECLSS components from 25 minutes. Before the AG begins to repair the ECLSS, the ECLSS begins to regulate the temperature and pressure with reduced efficiency as a result of damage. The time after the AG completely repairs the hole but before starting to repair the ECLSS, the air temperature and pressure behaviors across various repair sequences are identical. During the time of 15 to 25 minutes, the indoor temperature already returns to its initial conditions. This fast recovery occurs with the reduced efficiency of the ECLSS due to the low thermal capacity of the air resulting from the low air pressure. Variations in behavior occur when the AG starts its work. Variations in air pressure are more noticeable compared to the variation in air temperature across different repair sequences. This is because the air temperature returns to the setpoint even before the heating system is repaired and requires a small amount of thermal load to compensate for either heat loss or gain generated by heat and mass transfer with the interior wall surface temperature and supplied air. Since the required thermal load can be produced by damaged ECLSS, specifically cooling and heating systems, the variation is not dramatic. On the contrary, it takes a relatively longer time to regulate and return the air pressure to the setpoint, the bounceback duration in the air pressure varies depending on the repair sequence.

Performance curves of the air temperature and pressure can be generated using the temperature and pressure dataset. Fig. 15 and 16 illustrate two sets of performance curves based on specific habitat condition requirements for unmanned and manned mission periods, respectively. It is observed that variations in performance curves can occur even when using the same data set, as the curves are generated with different values of performance weight factors w_{r} based on the specified conditions provided in Table 2. The refined indoor air temperature and pressure criteria during manned missions, characterized by narrow acceptable temperature and pressure ranges, lead to more noticeable performance reductions compared to the curves during unmanned missions. Consequently, the minimum pressure performance value is zero during manned missions, while it is around 0.6 during unmanned missions. Conversely, the minimum

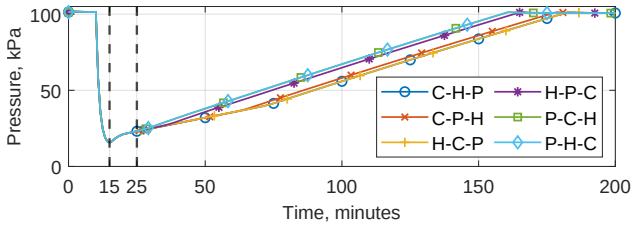

(a) Indoor air pressure behaviors.

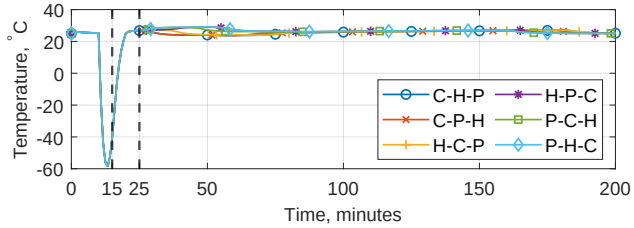

(b) Indoor air temperature behaviors.

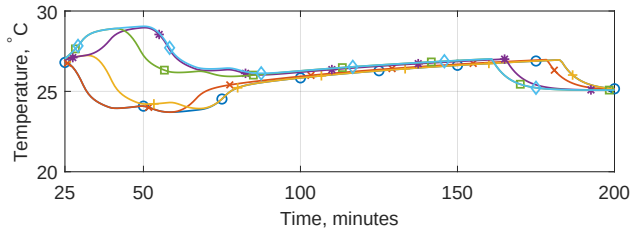

(c) Indoor air temperature behaviors (zoomed in).

Fig. 14 Habitat behaviors (state variables) across six different repair sequences (C: cooling system; H: heating system; P: IPCS).

temperature performance values drop to zero as the indoor air temperature falls below the lower limit of the warning range in both mission scenarios. Additionally, due to the low thermal capacity induced by the low pressure, the temperature performance rebounds to one before the AG initiates repairs to the damaged cooling and heating systems. Only small variations are observed across different repair sequences between 25 minutes and 60 minutes of simulation time during manned missions, as illustrated in Fig. 16. Consequently, the decrease in temperature performance is relatively less significant than the decrease in pressure performance. However, it is crucial to emphasize that this minor loss in temperature performance alone does not necessarily indicate that overall habitat conditions are within the acceptable range.

The final step in assessing resilience involves quantifying resilience values using different metrics and comparing the results to identify the most effective solution. In this case study, two resilience metrics are used: recovery resilience $\mathcal{R}_{\mathrm{r}}$ and resilience loss $\mathcal{R}_{\mathrm{loss}}$. $\mathcal{R}_{\mathrm{r}}$ represents the time taken for the system to return to its normal state after being damaged by a disruptive event, while $\mathcal{R}_{\mathrm{loss}}$ indicates the overall performance loss during the disruption duration, encompassing transient disruption, outage, and recovery periods. The results of each metric calculated during both unmanned and manned mission periods are shown in Figures 17 and 18, respectively. It is important to note that a more resilient system will exhibit lower values for both types of resilience metrics; a system is resilient if it can quickly recover from damage

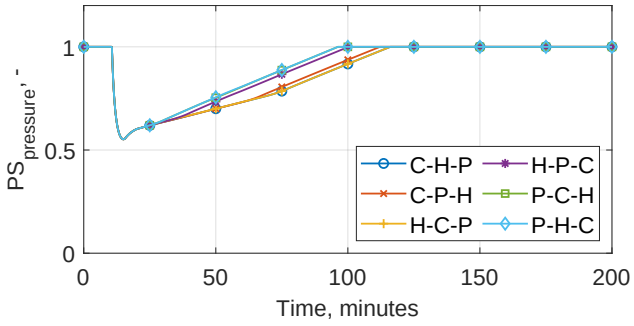

(a) Pressure performance.

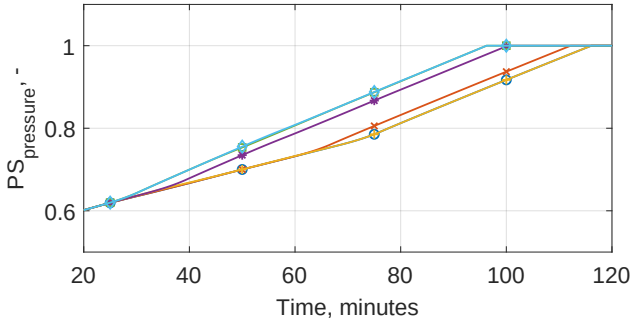

(b) Pressure performance (zoomed in).

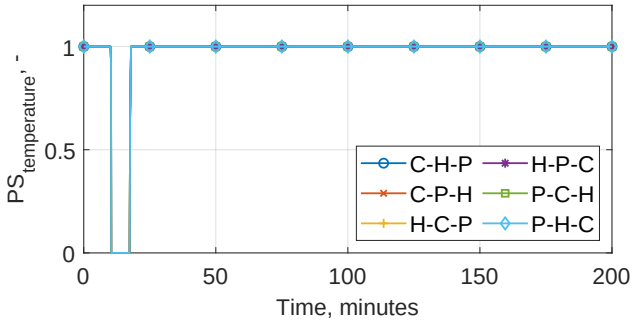

(c) Temperature performance.

Fig. 15 Habitat performance states across six different repair sequences during an unmanned mission.

with minimal overall performance loss over the evaluation period by involving repair actions.

Fig. 17 illustrates that the resilience value based on pressure performance is dominant in both types of metrics during unmanned mission periods, while the resilience of the temperature performance remains constant across different repair sequences. Furthermore, there is an inverse relationship between recovery resilience and resilience loss. The recovery resilience is at its lowest value with the "P-C-H" and "P-H-C" sequences, whereas the resilience loss is minimized with the "C-H-P" sequence. Since this analysis pertains to unmanned mission periods without a crew present in the habitat, it is preferable to have minimal performance loss ($\mathcal{R}_{\text{loss}}$) over an extended duration ($\mathcal{R}_{\text{r}}$). Therefore, the sequence "C-H-P" can be identified as the optimal solution for unmanned mission periods.

The results depicted in Fig. 18 exhibit more dynamic patterns. Resilience values for pressure and temperature demonstrate contrasting behaviors in both types of analyses. Additionally, the results of each analysis show opposite

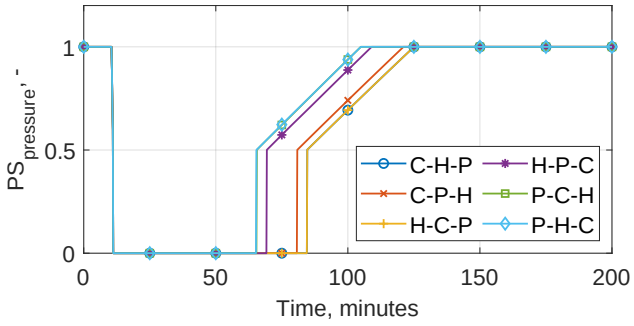

(a) Pressure performance.

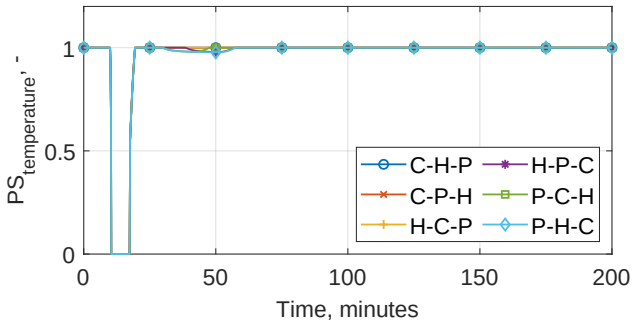

(b) Temperature performance.

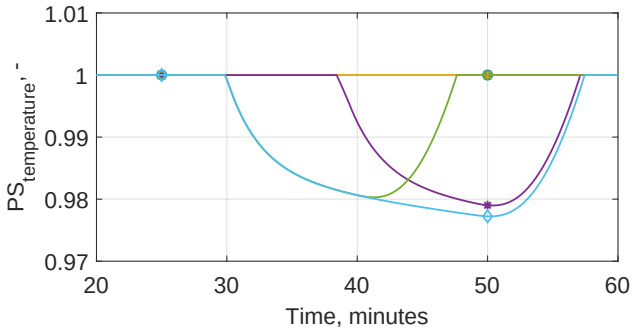

(c) Temperature performance (zoomed in).

Fig. 16 Habitat performance states across six different repair sequences during a manned mission.

trends. When determining the most suitable repair action based on these complex analysis results, it is essential to take into account the characteristics and requirements of the mission period. In manned mission periods, the primary consideration is the habitat conditions to ensure the well-being of the crew, with a focus on the crew's safety. In this context, pressure conditions take precedence over temperature conditions due to their immediate potential harm to the crew. Therefore, the resilience loss and recovery resilience of the pressure performance are of primary importance, while the resilience values of the temperature performance can serve as additional information for decision making. Moreover, a less pressure performance loss over an extended period is preferable to a sudden significant performance loss to ensure the crew's safety. Consequently, the potential optimal solutions are narrowed down to "C-H-P" and "H-C-P". Interestingly, these two candidates share the same values for recovery resilience $\mathcal{R}_r$ and resilience loss $\mathcal{R}_{loss}$ for temperature performance. This finding suggests that these two sequences could be considered the optimal repair

sequence during manned mission periods, necessitating additional quantification metrics involving other performance variables to determine the final optimal solution.

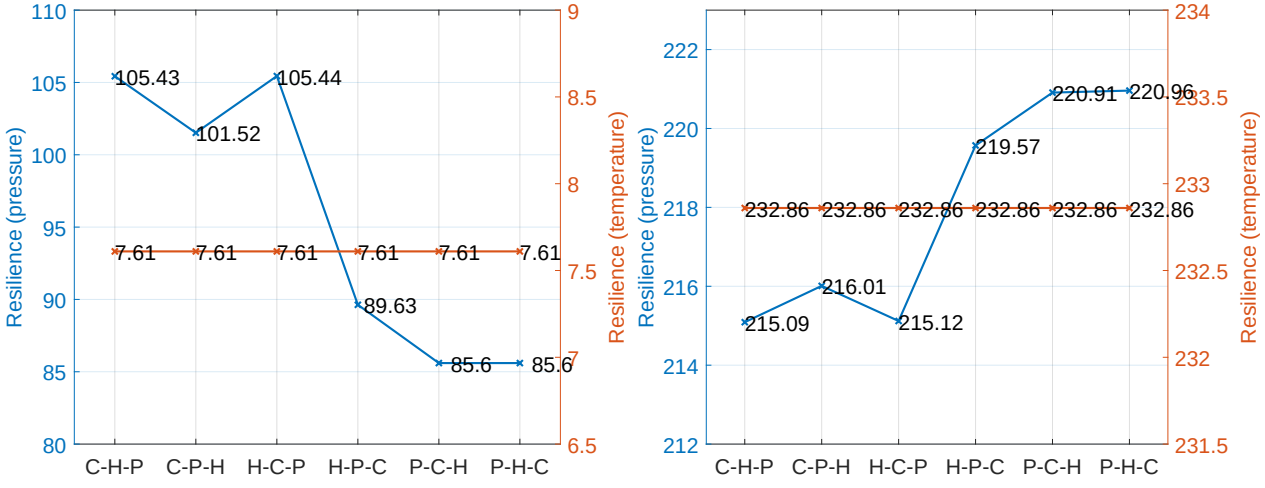

(a) Recovery resilience $\mathcal{R}_{\mathrm{r}}$. **(b) Resilience loss $\mathcal{R}_{\mathrm{loss}}$.**

Fig. 17 Resilience analysis during unmanned missions.

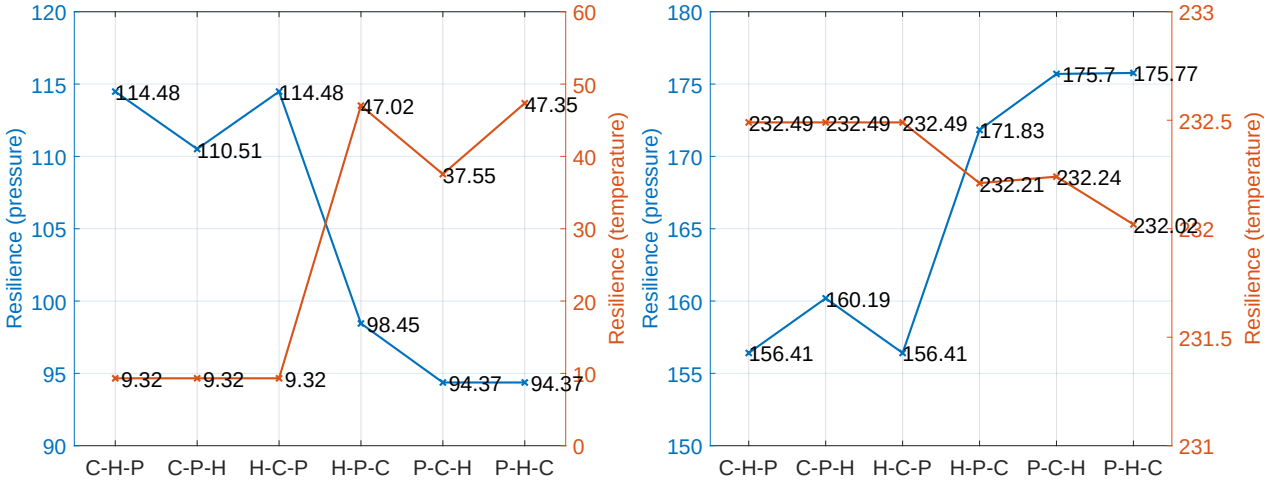

(a) Recovery resilience $\mathcal{R}_{\mathrm{r}}$. **(b) Resilience loss $\mathcal{R}_{\mathrm{loss}}$.**

Fig. 18 Resilience analysis during manned missions.

E. Discussion

In this section, a resilience-based investigation is carried out to determine the most effective sequence of the repair action for the damaged ECLSS components caused by a micrometeorite impact, showcasing the capabilities of the simulation model. Two state variables, indoor air temperature and pressure, are involved to assess different repair sequences based on the resilience quantification of habitat performances. The assessment considers two types of the mission periods, unmanned and manned, each with distinct habitat condition criteria. Through analyses of recovery

resilience and resilience loss, the "C-H-P" sequence is identified as the optimal solution for unmanned missions, whereas both the "C-H-P" and "H-C-P" sequences were considered suitable for manned mission periods.

This case study showcases the capability of HabSim to estimate complex dynamical behaviors of the lunar habitat at the component-, subsystem-, and habitat-level under the given conditions. The generated data set by HabSim with different repair sequences is used to conduct the resilience-based comparative analysis. Based on the measured resilience metrics, the optimal repair sequence is determined, which can reduce the overall risk to the habitat when it faces disruptive events, specifically a meteorite impact.

The case study demonstrates the potential contributions of HabSim to the proposed resilience evaluation framework that aims to support the resilience-oriented habitat design process. Accomplishing resilience analysis with different optimization objectives, such as system configurations and operating control strategies, under various disruptive events, decision-makers can design future resilient deep space habitats appropriately and prepare them for expected or unforeseen changes and disruptive events by reducing the risk rather than avoiding system failures. Additionally, it is shown that involving a multitude of state variables and various resilience metrics can enhance the rationality of the resilience assessment for deep space habitats.

V. Conclusion and Future Work

The importance of resilient deep space habitats for prolonged space exploration is widely acknowledged; however, detailed exploration of the design evaluation of the habitats, including their system configurations and operating strategies, remains limited. To address these gaps and challenges, this paper introduces a resilience-oriented habitat design evaluation framework. The evaluation framework consists of a deterministic structural-based deep space habitat simulator, which is developed by RETHi, and a resilience assessment based on habitat performances. An illustrative case study demonstrates the capabilities of the framework, specifically evaluating and identifying an optimal repair sequence for damaged ECLSS components based on resilience quantification. This case study shows that the proposed framework allows decision-makers to effectively analyze and assess habitat behaviors and performance under challenging space environment conditions and in response to disruptive events. Additionally, this research offers guidance for enhancing the resilient design of habitats during the early design phase.

The capability of the habitat simulator, which generates sufficiently realistic habitat behaviors, allows researchers to understand and investigate the performance of future habitats even before their deployment. However, the simulator also encompasses hypothetically designed disturbances (e.g., micrometeorite impacts, internal fire, etc.) which rely on strong assumptions. Calibrating the effects of these disturbances with experimental results or historical data from spacecrafts and the ISS can improve the reliability of the simulation results. Furthermore, resilience quantification is highly application-oriented; while various well-known generic resilience metrics exist, evaluations using these metrics may not adequately capture the unique characteristics of space habitats and their requirements. Thus, tailoring resilience

quantification to reflect the distinct features of space conditions and the requirements of space habitats can further enhance the credibility of the evaluation results.

Acknowledgments

This material is based upon work supported by NASA under grant or cooperative agreement award number 80NSSC19K1076 and Resilient Extra-Terrestrial Habitat Institute for Space Technology Research. In addition, the authors would like to acknowledge HabSim modelers for their contributions and Mohsen Azimi for coordinating all the collaborations.

References

[1] Harland, D. M., *The Story of Space Station Mir*, Springer Science & Business Media, 2007, Chap. 1, pp. 21–69. Google-Books-ID: sBdUh8WqEfYC.

[2] DeLucas, L. J., "International space station," *Acta Astronautica*, Vol. 38, 1996, pp. 613–619. https://doi.org/10.1016/0094-5765(96)00056-2, URL https://linkinghub.elsevier.com/retrieve/pii/0094576596000562.

[3] Kessler, P., Prater, T., Nickens, T., and Harris, D., "Artemis Deep Space Habitation: Enabling a Sustained Human Presence on the Moon and Beyond," *2022 Institute of Electrical and Electronics Engineers Aerospace Conference (AERO)*, Institute of Electrical and Electronics Engineers, 2022, pp. 1–12. https://doi.org/10.1109/AERO53065.2022.9843393, URL https://ieeexplore.ieee.org/document/9843393/.

[4] Leach, C., Dietlein, L., Pool, S., and Nicogossian, A., "Medical considerations for extending human presence in space," *Acta astronautica*, Vol. 21, No. 9, 1990, pp. 659–666. https://doi.org/10.1061/ASCEAS.1943-5525.0000054.

[5] Meng, C., Wang, W., Hao, Z., and Liu, H., "Investigation on the influence of isolated environment on human psychological and physiological health," *Science of The Total Environment*, Vol. 716, 2020, p. 136972. https://doi.org/https://doi.org/10.1016/j.scitotenv.2020.136972, URL https://www.sciencedirect.com/science/article/pii/S0048969720304824.

[6] Babayev, E. S., and Allahverdiyeva, A. A., "Effects of geomagnetic activity variations on the physiological and psychological state of functionally healthy humans: Some results of Azerbaijani studies," *Advances in Space Research*, Vol. 40, 2007, pp. 1941–1951. https://doi.org/10.1016/J.ASR.2007.02.099.

[7] Brooks, R. A., Maes, P., Mataric, M. J., and More, G., "Lunar base construction robots," *Institute of Electrical and Electronics Engineers International Workshop on Intelligent Robots and Systems, Towards a New Frontier of Applications*, Institute of Electrical and Electronics Engineers, 1990, pp. 389–392. https://doi.org/10.1109/IROS.1990.262415, URL http://ieeexplore.ieee.org/document/262415/.

[8] Ruess, F., Schaenzlin, J., and Benaroya, H., "Structural design of a lunar habitat," *Journal of Aerospace Engineering*, Vol. 19, No. 3, 2006, pp. 133–157. https://doi.org/10.1061/(ASCE)0893-1321(2006)19:3(133), URL https://ascelibrary.org/doi/abs/10.1061/%28ASCE%290893-1321%282006%2919%3A3%28133%29.

[9] Hegde, U., Balasubramaniam, R., and Gokoglu, S., "Analysis of Water Extraction from Lunar Regolith," *50th AIAA Aerospace Sciences Meeting including the New Horizons Forum and Aerospace Exposition*, American Institute of Aeronautics and Astronautics, 2012. https://doi.org/10.2514/6.2012-634, URL https://arc.aiaa.org/doi/10.2514/6.2012-634.

[10] Schwandt, C., Hamilton, J. A., Fray, D. J., and Crawford, I. A., "The production of oxygen and metal from lunar regolith," *Planetary and Space Science*, Vol. 74, 2012, pp. 49–56. https://doi.org/10.1016/j.pss.2012.06.011, URL https://linkinghub.elsevier.com/retrieve/pii/S0032063312001821.

[11] Jaumann, R., Hiesinger, H., Anand, M., Crawford, I. A., Wagner, R., Sohl, F., Jolliff, B. L., Scholten, F., Knapmeyer, M., Hoffmann, H., Hussmann, H., Grott, M., Hempel, S., Köhler, U., Krohn, K., Schmitz, N., Carpenter, J., Wieczorek, M., Spohn, T., Robinson, M. S., and Oberst, J., "Geology, geochemistry, and geophysics of the Moon: Status of current understanding," *Planetary and Space Science*, Vol. 74, 2012, pp. 15–41. https://doi.org/10.1016/j.pss.2012.08.019, URL https://linkinghub.elsevier.com/retrieve/pii/S0032063312002565.

[12] Escobar-Cerezo, J., Penttilä, A., Kohout, T., Muñoz, O., Moreno, F., and Muinonen, K., "Simulations of Effects of Nanophase Iron Space Weather Products on Lunar Regolith Reflectance Spectra," *The Astrophysical Journal*, Vol. 853, 2018, p. 71. https://doi.org/10.3847/1538-4357/aaa24d, URL https://iopscience.iop.org/article/10.3847/1538-4357/aaa24d.

[13] Plainaki, C., Lilensten, J., Radioti, A., Andriopoulou, M., Milillo, A., Nordheim, T. A., Dandouras, I., Coustenis, A., Grassi, D., Mangano, V., Massetti, S., Orsini, S., and Lucchetti, A., "Planetary space weather: scientific aspects and future perspectives," *Journal of Space Weather and Space Climate*, Vol. 6, 2016, p. A31. https://doi.org/10.1051/swsc/2016024, URL http://www.swsc-journal.org/10.1051/swsc/2016024.

[14] Austin, A., Sherwood, B., Elliott, J., Colaprete, A., Zacny, K., Metzger, P., Sims, M., Schmitt, H., Magnus, S., Fong, T., Smith, M., Casillas, R. P., Howe, A. S., Voecks, G., Vaquero, M., and Vendiola, V., "Robotic Lunar Surface Operations 2," *Acta Astronautica*, Vol. 176, 2020, pp. 424–437. https://doi.org/10.1016/j.actaastro.2020.06.038, URL https://linkinghub.elsevier.com/retrieve/pii/S0094576520304057.

[15] Sherwood, B., "Principles for a practical Moon base," *Acta Astronautica*, Vol. 160, 2019, pp. 116–124. https://doi.org/10.1016/j.actaastro.2019.04.018, URL https://linkinghub.elsevier.com/retrieve/pii/S0094576518319593.

[16] Akimov, E. V., Kozorez, D. A., and Kruzhkov, D. M., "Navigation Solution Concept and Its Practical Approach Development for Lunar Missions," *Russian Engineering Research*, Vol. 40, 2020, pp. 605–607. https://doi.org/10.3103/S1068798X20070035.

[17] Smith, M., Craig, D., Herrmann, N., Mahoney, E., Krezel, J., McIntyre, N., and Goodliff, K., "The Artemis Program: An Overview of NASA's Activities to Return Humans to the Moon," *2020 Institute of Electrical and Electronics Engineers Aerospace Conference*, Institute of Electrical and Electronics Engineers, 2020, pp. 1–10. https://doi.org/10.1109/AERO47225.2020.9172323, URL https://ieeexplore.ieee.org/document/9172323/.

[18] White, B. E., "Fostering intra-organizational communication of enterprise systems engineering practices," *National Defense Industrial Association, 9th Annual Systems Engineering Conference*, Citeseer, San Diego, CA, 2006, pp. 22–26.

[19] Uday, P., and Marais, K., "Designing Resilient Systems-of-Systems: A Survey of Metrics, Methods, and Challenges," *Systems Engineering*, Vol. 18, 2015, pp. 491–510. https://doi.org/10.1002/sys.21325, URL https://incose.onlinelibrary.wiley.com/doi/10.1002/sys.21325.

[20] DeLaurentis, D. A., Crossley, W. A., and Mane, M., "Taxonomy to Guide Systems-of-Systems Decision-Making in Air Transportation Problems," *Journal of Aircraft*, Vol. 48, 2011, pp. 760–770. https://doi.org/10.2514/1.C031008, URL https://arc.aiaa.org/doi/10.2514/1.C031008.

[21] Azimi, M., Lund, A., Fu, Y., Montoya, H., Vaccino, L., Krishnan, M., Rhee, S., Chebbo, L., Shahriar, A., Wang, Z., Maghareh, A., and Dyke, S., "HabSim: A Modular Coupled Virtual Testbed for Simulating ExtraTerrestrial Habitat Systems," *AIAA Journal*, 2024. In review.

[22] Sakatani, N., Ogawa, K., Arakawa, M., and Tanaka, S., "Thermal conductivity of lunar regolith simulant JSC-1A under vacuum," *Icarus*, Vol. 309, 2018, pp. 13–24. https://doi.org/https://doi.org/10.1016/j.icarus.2018.02.027, URL https://www.sciencedirect.com/science/article/pii/S0019103517308023.

[23] Gentry, G. J., and Cover, J., "International space station (ISS) environmental control and life support (ECLS) system overview of events: 2010-2014," *International Conference on Environmental Systems (ICES)*, 2015.

[24] Joshi, A., Korn, C., Magkos, M., Amara, Y., Anil, A., Bhattacherjee, S., Dargent de Vicente, S., Haffmans, P., Heinz, N., Hinkel, A., et al., "AMORE-Mission concept overview for a progressively independent and self-sustainable lunar habitat," *4th Symposium on Space Educational Activities*, Universitat Politècnica de Catalunya, Universitat Politècnica de Catalunya, 2022, pp. 407–412. https://doi.org/10.5821/conference-9788419184405.071.

[25] Jablonski, A. M., and Ogden, K. A., "Technical requirements for lunar structures," *Journal of Aerospace Engineering*, Vol. 21, No. 2, 2008, pp. 72–90. https://doi.org/10.1061/ASCE0893-1321200821:272, URL https://ascelibrary.org/doi/abs/10.1061/%28ASCE%290893-1321%282008%2921%3A2%2872%29.

[26] Castet, J.-F., and Saleh, J., "Survivability and resiliency of spacecraft and space-based networks: a framework for characterization and analysis," *AIAA Space 2008 Conference & Exposition*, 2008, p. 7707.

[27] Gu, X., Jin, X., Ni, J., and Koren, Y., "Manufacturing System Design for Resilience," *Procedia CIRP*, Vol. 36, 2015, pp. 135–140. https://doi.org/10.1016/j.procir.2015.02.075, URL https://linkinghub.elsevier.com/retrieve/pii/S2212827115001183.

[28] Balchanos, M. G., Kashani-Pour, A. R., Thakker, A., Kwan, H., and Vivanco, S., "Resilient Autonomous Systems: Life-Cycle Design, Metrics and Simulation-based Assessment," *2018 AIAA Aerospace Sciences Meeting*, American Institute of Aeronautics and Astronautics, 2018. https://doi.org/10.2514/6.2018-1215, URL https://arc.aiaa.org/doi/10.2514/6.2018-1215.

[29] Moslehi, S., and Reddy, T. A., "Sustainability of integrated energy systems: A performance-based resilience assessment methodology," *Applied Energy*, Vol. 228, 2018, pp. 487–498. https://doi.org/10.1016/j.apenergy.2018.06.075, URL https://linkinghub.elsevier.com/retrieve/pii/S0306261918309401.

[30] Matelli, J. A., and Goebel, K., "Resilience evaluation of the environmental control and life support system of a spacecraft for deep space travel," *Acta Astronautica*, Vol. 152, 2018, pp. 360–369. https://doi.org/10.1016/j.actaastro.2018.08.045, URL https://linkinghub.elsevier.com/retrieve/pii/S0094576518310518.

[31] Xing, P., Huixiong, W., Yanjing, Y., and Guozhong, Z., "Resilience based importance measure analysis for SoS," *Journal of Systems Engineering and Electronics*, Vol. 30, No. 5, 2019, pp. 920–930. https://doi.org/10.21629/JSEE.2019.05.10.

[32] Zhang, C., Kazanci, O. B., Levinson, R., Heiselberg, P., Olesen, B. W., Chiesa, G., Sodagar, B., Ai, Z., Selkowitz, S., Zinzi, M., Mahdavi, A., Teufl, H., Kolokotroni, M., Salvati, A., Bozonnet, E., Chtioui, F., Salagnac, P., Rahif, R., Attia, S., Lemort, V., Elnagar, E., Breesch, H., Sengupta, A., Wang, L. L., Qi, D., Stern, P., Yoon, N., Bogatu, D.-I., Rupp, R. F., Arghand, T., Javed, S., Akander, J., Hayati, A., Cehlin, M., Sayadi, S., Forghani, S., Zhang, H., Arens, E., and Zhang, G., "Resilient cooling strategies – A critical review and qualitative assessment," *Energy and Buildings*, Vol. 251, 2021, p. 111312. https://doi.org/10.1016/j.enbuild.2021.111312, URL https://linkinghub.elsevier.com/retrieve/pii/S037877882100596X.

[33] Cimellaro, G. P., Reinhorn, A. M., and Bruneau, M., "Framework for analytical quantification of disaster resilience," *Engineering Structures*, Vol. 32, No. 11, 2010, pp. 3639–3649. https://doi.org/10.1016/j.engstruct.2010.08.008, URL https://linkinghub.elsevier.com/retrieve/pii/S014102961000297X.

[34] Henry, D., and Ramirez-Marquez, J. E., "Generic metrics and quantitative approaches for system resilience as a function of time," *Reliability Engineering & System Safety*, Vol. 99, 2012, pp. 114–122. https://doi.org/10.1016/j.ress.2011.09.002, URL https://linkinghub.elsevier.com/retrieve/pii/S0951832011001748.

[35] Adjetey-Bahun, K., Birregah, B., Châtelet, E., and Planchet, J.-L., "A model to quantify the resilience of mass railway transportation systems," *Reliability Engineering & System Safety*, Vol. 153, 2016, pp. 1–14. https://doi.org/https://doi.org/10.1016/j.ress.2016.03.015, URL https://www.sciencedirect.com/science/article/pii/S0951832016300059.

[36] Rines, M. R., Balchanos, M., Mavris, D. N., Rao, J., and Williams, J., *A Resource Allocation Algorithm for a Space Habitat ECLSS*, AIAA, 2021, p. 4028. https://doi.org/10.2514/6.2021-4028, URL https://arc.aiaa.org/doi/abs/10.2514/6.2021-4028.

[37] Abbasnejadfard, M., Bastami, M., Abbasnejadfard, M., and Borzoo, S., "Novel deterministic and probabilistic resilience assessment measures for engineering and infrastructure systems based on the economic impacts," *International Journal of Disaster Risk Reduction*, Vol. 75, 2022, p. 102956. https://doi.org/10.1016/j.ijdrr.2022.102956, URL https://linkinghub.elsevier.com/retrieve/pii/S2212420922001753.

[38] Dyke, S. J., Marais, K., Bilionis, I., Werfel, J., and Malla, R., "Strategies for the design and operation of resilient extraterrestrial habitats," *Sensors and Smart Structures Technologies for Civil, Mechanical, and Aerospace Systems 2021*, edited by D. Zonta, H. Huang, and Z. Su, SPIE, 2021, p. 2. https://doi.org/10.1117/12.2585118, URL https://www.spiedigitallibrary.org/conference-proceedings-of-spie/11591/2585118/Strategies-for-the-design-and-operation-of-resilient-extraterrestrial-habitats/10.1117/12.2585118.full.

[39] MATLAB, *version 9.8.0 (R2020a)*, The MathWorks Inc., Natick, Massachusetts, 2020.

[40] Rhee, S., Noble, Z., Park, J., Lial, A., Collazo, C. L., and Davide, Z., "Development of a Damageable ECLSS and Interior-Environment Virtual Testbed Model to Simulate Future Resilient Deep Space Habitats," *The 52nd International Conference on Environmental Systems*, 2023 International Conference on Environmental Systems, Calgary, AB, 2023. URL https://hdl.handle.net/2346/94628.

[41] Vivian, J., Zarrella, A., Emmi, G., and De Carli, M., "An evaluation of the suitability of lumped-capacitance models in calculating energy needs and thermal behavior of buildings," *Energy and Buildings*, Vol. 150, 2017, pp. 447–465. https://doi.org/https://doi.org/10.1016/j.enbuild.2017.06.021.

[42] Oliveira Panão, M. J., Santos, C. A., Mateus, N. M., and Carrilho da Graça, G., "Validation of a lumped RC model for thermal simulation of a double skin natural and mechanical ventilated test cell," *Energy and Buildings*, Vol. 121, 2016, pp. 92–103. https://doi.org/https://doi.org/10.1016/j.enbuild.2016.03.054, URL https://www.sciencedirect.com/science/article/pii/S0378778816302109.

[43] Bourgeois, T., Ammouri, F., Weber, M., and Knapik, C., "Evaluating the temperature inside a tank during a filling with highly-pressurized gas," *international journal of hydrogen energy*, Vol. 40, No. 35, 2015, pp. 11748–11755. https://doi.org/https://doi.org/10.1016/j.ijhydene.2015.01.096.

[44] Bendapudi, S., Braun, J. E., and Groll, E. A., "A comparison of moving-boundary and finite-volume formulations for transients in centrifugal chillers," *International journal of refrigeration*, Vol. 31, No. 8, 2008, pp. 1437–1452. https://doi.org/https://doi.org/10.1016/j.ijrefrig.2008.03.006.

[45] Pan, C., Ziviani, D., and Braun, J. E., "Performance evaluation of a vapor-compression-cycle based heat pump system for a lunar habitat under the impact of dust deposits on the coupled radiators," *Acta Astronautica*, Vol. 194, 2022, pp. 22–33. https://doi.org/https://doi.org/10.1016/j.actaastro.2022.01.040.

[46] Sridhar, K., Gottmann, M., and Nanjundan, A., "Thermal control systems for low-temperature heat rejection on a lunar base," Tech. rep., NASA, 1993.

[47] Hanford, A. J., and Ewert, M. K., "Advanced active thermal control systems architecture study," Tech. rep., NASA, 1996.

[48] Moore, K. C., "Design and Performance of the Space Station Pressure Control Assembly," *SAE Transactions*, Vol. 105, 1996, pp. 1078–1106. URL http://www.jstor.org/stable/44725601.

[49] Williams, J.-P., Paige, D., Greenhagen, B., and Sefton-Nash, E., "The global surface temperatures of the Moon as measured by the Diviner Lunar Radiometer Experiment," *Icarus*, Vol. 283, 2017, pp. 300–325. https://doi.org/https://doi.org/10.1016/j.icarus.2016.08.012.

[50] Ulmer, J., "A Resilience-Oriented Extra-Terrestrial Habitat Design Process," Ph.D. thesis, Purdue University, 2023.

[51] Nan, C., and Sansavini, G., "A quantitative method for assessing resilience of interdependent infrastructures," *Reliability Engineering & System Safety*, Vol. 157, 2017, pp. 35–53. https://doi.org/https://doi.org/10.1016/j.ress.2016.08.013.

[52] Moazami, A., Carlucci, S., and Geving, S., "Robust and resilient buildings: A framework for defining the protection against climate uncertainty," *IOP Conference Series: Materials Science and Engineering*, Vol. 609, 2019, p. 72068. https://doi.org/10.1088/1757-899X/609/7/072068, URL https://iopscience.iop.org/article/10.1088/1757-899X/609/7/072068.

[53] Umunnakwe, A., Huang, H., Oikonomou, K., and Davis, K. R., "Quantitative analysis of power systems resilience: Standardization, categorizations, and challenges," *Renewable and Sustainable Energy Reviews*, Vol. 149, 2021, p. 111252. https://doi.org/10.1016/j.rser.2021.111252, URL https://linkinghub.elsevier.com/retrieve/pii/S1364032121005396.

[54] Yodo, N., and Wang, P., "Engineering Resilience Quantification and System Design Implications: A Literature Survey," *Journal of Mechanical Design*, Vol. 138, No. 11, 2016, p. 111408. https://doi.org/10.1115/1.4034223, URL https://doi.org/10.1115/1.4034223.

[55] Munoz, A., and Dunbar, M., "On the quantification of operational supply chain resilience," *International Journal of Production Research*, Vol. 53, 2015, pp. 6736–6751. https://doi.org/10.1080/00207543.2015.1057296, URL http://www.tandfonline.com/doi/full/10.1080/00207543.2015.1057296.

[56] Das, L., Munikoti, S., Natarajan, B., and Srinivasan, B., "Measuring smart grid resilience: Methods, challenges and opportunities," *Renewable and Sustainable Energy Reviews*, Vol. 130, 2020, p. 109918. https://doi.org/10.1016/j.rser.2020.109918, URL https://linkinghub.elsevier.com/retrieve/pii/S1364032120302094.

[57] Gerstenmaier, W. H., Parker, D., Leclerc, G., and Shirama, R., "International Environmental Control and Life Support System Interoperability Standards (IECLSSIS)," , 2019. URL https://nasasitebuilder.nasawestprime.com/wp-content/uploads/sites/45/2019/09/eclss_baseline_final_3-2019.pdf.

[58] Abraini, J., David, H., Vallée, N., and Risso, J.-J., "Theoretical considerations on the ultimate depth that could be reached by saturation human divers," *Medical Gas Research*, Vol. 6, 2016, p. 119. https://doi.org/10.4103/2045-9912.184722, URL https://journals.lww.com/10.4103/2045-9912.184722.

[59] Ebi, K. L., Capon, A., Berry, P., Broderick, C., de Dear, R., Havenith, G., Honda, Y., Kovats, R. S., Ma, W., Malik, A., Morris, N. B., Nybo, L., Seneviratne, S. I., Vanos, J., and Jay, O., "Hot weather and heat extremes: health risks," *The Lancet*, Vol. 398, 2021, pp. 698–708. https://doi.org/10.1016/S0140-6736(21)01208-3, URL https://linkinghub.elsevier.com/retrieve/pii/S0140673621012083.